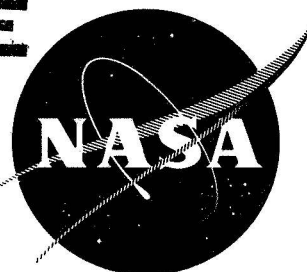N 70 17 29 8

NASA CR-72622

CASE FILE COPY

NASA

BIPROPELLANT DROPLET BURNING RATES AND LIFETIMES IN A COMBUSTION GAS ENVIRONMENT

by

G. M. Faeth and R. S. Lazar

prepared for

Mechanical Engineering Department
The Pennsylvania State University
University Park, Pa.

NASA CR-72622

BIPROPELLANT DROPLET BURNING RATES AND
LIFETIMES IN A COMBUSTION GAS ENVIRONMENT

by

G. M. Faeth and R. S. Lazar

prepared for

National Aeronautics and Space Administration

December 1, 1969

Contract NGR 39-009-077

Technical Management
NASA Lewis Research Center
Cleveland, Ohio

Chemical Rockets Division

R. J. Priem

Department of Mechanical Engineering
The Pennsylvania State University
University Park, Pennsylvania

BIPROPELLANT DROPLET BURNING RATES AND

LIFETIMES IN A COMBUSTION GAS ENVIRONMENT

by

G. M. Faeth and R. S. Lazar

ABSTRACT

Measurements of droplet heat-up and steady burning were made at atmospheric pressure with a flat flame burner apparatus. Various alcohols and paraffin hydrocarbons were tested at ambient temperatures of 1660 - 2530° K and ambient oxygen concentrations in the range 0 - 38%. Existing diffusion flame theories of droplet combustion gave an adequate prediction of the measured influence of ambient oxygen concentration and temperature, but showed progressive failure for the heavier hydrocarbons. Flame luminosity was observed very early in the heat-up period. The steady burning theory was extended to include the heat-up period and theoretical and experimental comparisons were made over the entire droplet lifetime with results roughly the same as the steady burning results.

TABLE OF CONTENTS

BIPROPELLANT DROPLET BURNING RATES AND
LIFETIMES IN A COMBUSTION GAS ENVIRONMENT

by

G. M. Faeth and R. S. Lazar
The Pennsylvania State University

Summary

The work described in this report considers the burning characteristics of liquid fuel droplets in a combustion gas environment at atmospheric pressure. The fuels considered in the study included methyl, 1-butyl and 1-decyl alcohol as well as the paraffin hydrocarbons, n-pentane, n-heptane, n-octane, iso-octane, n-decane, n-tridecane, and n-hexadecane.

The test droplets were mounted on a probe and rapidly subjected to the combustion products of a flat flame burner in order to simulate a combustion chamber environment. The burner provided ambient temperatures in the range 1660 - 2530°K and ambient oxygen concentrations in the range 0 - 38% at the droplet location. Existing steady burning theories were extended to the heat-up period allowing comparison with the experimental results for both steady burning rates and droplet life histories.

The conclusions of the study are as follows:

1. Over the entire range of testing, the simplified diffusion flame theory gave reasonable agreement with the experimental results with maximum errors on the order of 40% for droplet burning rates.

2. The trends of the burning rate with respect to ambient temperature and oxygen concentration were predicted reasonably well over the test range.

3. All theoretical methods progressively overestimate the burning rate as the molecular weight of the fuel is increased. This failure is attributed to fuel decomposition in the region between the droplet surface and the oxidation zone.

4. Flame luminosity was observed early in the heat-up period (on the order of 10 to 20% of the heat-up time). This allowed the use of a quasisteady combustion model throughout the lifetime of a droplet for these high temperature conditions.

5. Errors in droplet life histories were found to be about the same as those for steady burning rates. The extended model gave a reasonably good prediction of the influence of combustion on the drop-let heat-up time.

6. The simplified, constant property analysis was compared with a very realistic variable property solution for the case of droplet evaporation without combustion. Differences between the two methods were less than 6%.

LIST OF FIGURES

LIST OF TABLES

NOMENCLATURE

a, b	Constants in specific heat approximation, Eq. (44)
$C_1, \cdots, C_7$	Constants defined in Appendix A
C_p, C_{p_ℓ}	Gas and liquid specific heat
C_{pR}	Dimensionless parameter, Eq. (19)
d_ℓ	Droplet diameter
D	Effective binary diffusivity
D_{ij}	Binary diffusivity of i with respect to j
h	Heat transfer coefficient
h_i	enthalpy of species i
h_{fg}	Heat of vaporization
h_i°	Enthalpy of formation of gaseous species i
H_c	Heat of reaction
i	lbm of oxidant per lbm of fuel
k	Reaction rate constant
K	Burning rate constant, Eq. (38)
L	Lewis number, Eq. (20)
m	Droplet mass
$\dot{m}$	Mass flux per unit solid angle
$\dot{M}$	Molal droplet evaporation rate
p	Pressure
Pe	Peclet number $= RePr$

Pr	Prandtl number $= C_p \mu / \lambda$
P_v	Vapor pressure
$\dot{q}$	Energy flux per unit solid angle
Q_R	Dimensionless heat of reaction, Eq. (21)
r	Radial Distance
r_ℓ, r_f	Droplet and flame radius
Re	Reynold's number $= \rho d_\ell V_\infty / \mu$
R_u	Universal gas constant
Sc	Schmidt number $= \mu / \rho D$
t	Time
T	Temperature
Tc	Critical temperature
T_R	Reduced temperature $= T/T_c$
V_∞	Gas velocity
W	Molecular weight
X_i	Mole fraction of species i
Y_i	Mass fraction of species i
ε_i	Mass flux of species i
λ	Thermal conductivity
μ	Viscosity
ξ	Parameter, Eq. (46)
ρ, ρ_ℓ	Gas and liquid density

ϕ Dimensionless parameter, Eq. (12)

Subscripts and Superscripts

A,B	Regions A and B
f	At flame
F	Fuel
ℓ	At droplet
VP	Variable property
P	Product
X	Oxidant
0	Initial value
∞	At infinity
*	No convection effects

INTRODUCTION

Due to its importance as an elemental process in spray combustion systems, many investigators have studied the burning of single fuel droplets. The bulk of these studies were conducted by burning droplets at low ambient temperatures, with oxygen concentrations ranging from air to pure oxygen.[1-5] However, since the ambient environment of these tests is so different from the environment of droplets in a combustion chamber, the results must be extrapolated to reach the range of practical combustion systems.

Wood, et al,[6] have presented a study that is more relevant to combustion chambers. These investigators considered the combustion of hexadecane, kerosene, and various heating oils within a premixed flame. Droplet burning was observed for oxygen mass fractions in the range 0 - .81, while maintaining a constant ambient temperature of 1775°K around the droplet. Average burning rate constants were inferred from measurements of initial droplet diameter and the total time of combustion luminosity.

The accuracy of the burning rate measurements of Ref. (6) is questionable, since the heat-up period is combined with the steady burning period. This tends to underestimate the true burning rate constant of the droplet. Furthermore, the end of luminosity occurs some time after the droplet has completely evaporated, adding additional uncertainties to the burning rate measurement.

In view of these objections, the present study was undertaken to provide a more accurate measurement of droplet combustion at high ambient temperatures. Another objective of the present study was to extend the range of hydrocarbons and ambient temperatures from that of Ref. (6), in order to provide a more stringent test of the droplet combustion models.

In the experiments, test droplets were rapidly immersed in the combustion products of a flat flame burner, in order to simulate the injection of a droplet into a combustion chamber. The burner was operated at atmospheric pressure

with various initial gas compositions to yield temperatures in the range 1660 - 2530°K and oxygen mass fractions of 0 - .38 at the test droplet location. The droplet fuels considered in the study included methyl, 1-butyl, and 1-decyl alcohol as well as the paraffin hydrocarbons, n-pentane, n-heptane, n-octane, iso-octane, n-decane, n-tridecane, and n-hexadecane.

The bulk of the testing involved burning rate measurements at the wet bulb state of the droplet. Limited results were also obtained on droplet lifetimes and the time when luminosity appeared following the immersion of the droplet in the hot burner gas. The steady burning theories of Refs. (1 - 6) were extended to include the presence of an active combustion zone during the heat-up period of the droplet. The expanded theory was then employed to compute droplet life histories for comparison with the data.

APPARATUS

A sketch of the experimental apparatus is shown in Fig. 1. The flat flame burner was mounted on rails so that it could be rapidly moved under the droplet location with a solenoid valve actuated pneumatic cylinder. The burner face was 5 cm. in diameter and in the test position (illustrated in Fig. 1) the droplet was 1 cm. above the center of the burner. The time between the droplet first entering the burner flame and the burner coming to rest in the test position was on the order of 10 ms.

The flat flame burner was similar to the one described by Friedman and Macek.[7] The burner was operated with various mixtures of carbon monoxide, hydrogen, oxygen, and nitrogen (commercial grade). The flow of these gases was measured with rotameters which were calibrated with a wet test meter. The heat loss from the burner flame to the face of the burner was determined by measuring the temperature rise and flow rate of the burner cooling water.

The temperature and composition of the burned gas flowing around the droplet was determined from thermochemical calculations allowing for all relevant dissociation reactions and heat loss to the burner. The thermochemical properties for these calculations were taken from the JANAF tables.[8] The gas velocity at the droplet location was calculated from the mass flux into the burner and the known properties of the burned gas. This procedure is adequate since the test position is well within the potential core of the jet leaving the burner. Table I summarizes the computed properties of the gas stream at the droplet location, for the test conditions employed in the present study.

The test droplet was mounted on a quartz filament having a diameter of approximately 100μ. The bottom end of the probe was slightly enlarged to aid in supporting the droplet.
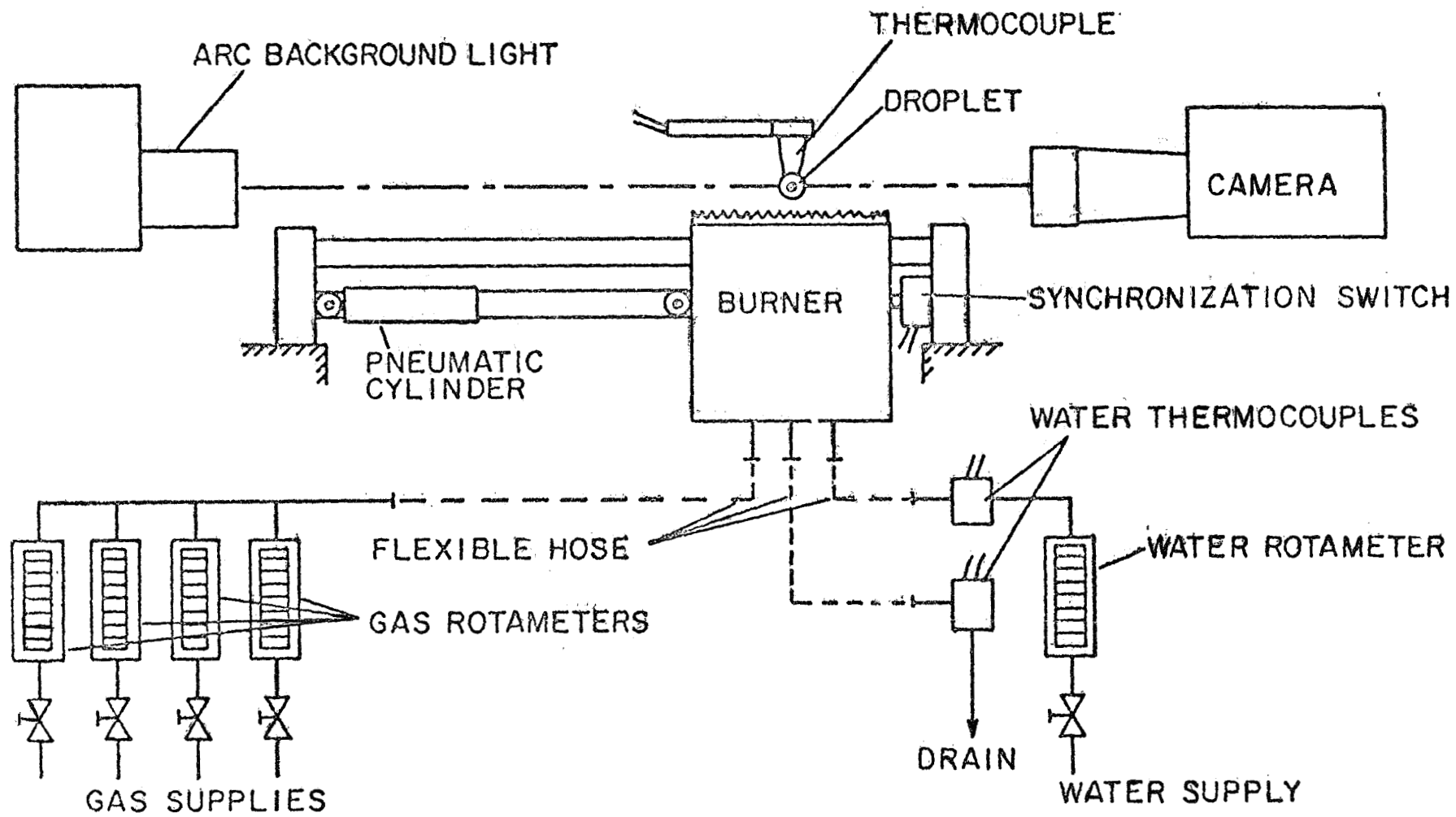
Fig. 1   Sketch of the Experimental Apparatus.

4

TABLE I: PROPERTIES OF THE AMBIENT GAS FOR VARIOUS TEST CONDITIONS

Y_x	T_∞ °K	V_∞ cm/sec	PRODUCT MOLE FRACTION							
			CO	CO_2	H_2	H_2O	NO	N_2	O	O_2
.046	2530	62.5	.099	.415	0	0	.009	.430	.004	.043
.138	↓	↓	.058	.439	↓	↓	.014	.339	.007	.143
.227			.041	.423			.017	.270	.009	.240
.308			.033	.402			.016	.208	.011	.330
.371	↓	↓	.022	.381			.015	.172	.009	.401
0	2350	46.7	.288	.427			0	.285	0	0
0	2220		.251	.374	↓	↓		.375		
0	2060		.371	.429	.029	.171		0		
0	1830		.294	.353	.029	.134		.190		
0	1660	↓	.245	.296	.026	.109	↓	.324	↓	↓

Droplet diameters were measured from shadowgraphs recorded by a 16mm cine camera operating at speeds on the order of 100 pictures per second. The elliptical shape of the droplet was corrected to a sphere of equal volume as discussed by Kobayasi.[9]

Dark field photographs were also made with a second cine camera operating at speeds on the order of 150 pictures per second in order to measure the time of appearance of combustion luminosity. Both cameras were electrically driven with internal timing lights driven with a 100 cps signal generator.

ANALYSIS

Many theories of droplet combustion have been limited to steady burning at the wet bulb state.[1-4] The wet bulb state is the condition where all the energy reaching the droplet is utilized for the heat of vaporization of the material evaporating from the droplet and the liquid temperature remains constant. In order to compute the entire life history of a droplet, transport rates must also be estimated during the heat-up period where the droplet temperature increases from its initial value to the wet bulb temperature. The following analysis will consider the extension of the steady burning theories to the heat-up period.

For the analysis, the gas phase combustion zone around the droplet was assumed to be quasisteady, i.e., the combustion zone adjusts rapidly to the changing boundary conditions at the surface of the droplet. This assumption is valid under conditions where the characteristic transient time of the gas phase, r_ℓ^2/D, is small in comparison with the lifetime of the droplet.[10] This requirement was easily satisfied for the conditions of the present experiments and is a common assumption for droplet lifetime calculations under combustion chamber conditions.[11]

The quasisteady assumption decouples the gas phase problem from the transient solution at the droplet. Therefore, in the following, the gas phase is solved for general boundary conditions and these results are then applied to the conservation relations at the droplet in order to compute the time variation of droplet diameter and temperature.

Gas Phase Analysis: The initial formulation of the gas phase problem is made under the assumption of spherical symmetry, in the absence of convection. Corrections for convection will be considered following the initial development of the equations.

The theoretical model is illustrated in Fig. 2. Fuel and oxidizer are assumed to meet and react in an infinitely thin reaction zone concentric with the droplet surface. No consideration is made of fuel or oxidizer decomposition prior to these components reacting at the flame surface.

With respect to gas properties, ideal gases are assumed and only concentration diffusion is considered. Quadratic velocity terms and radial pressure gradients are neglected. In region A, interior to the reaction zone, it is assumed that there is a binary mixture of fuel vapor and product gas (considered to be a single species). The gas exterior to the reaction zone, region B, is assumed to be a binary mixture of oxidizer and the product gas.

Under these assumptions, and with all reaction limited to the flame surface, the general gas phase conservation relations given by Williams[12] take the following form:

$$\frac{d}{dr}(\dot{m}) = \frac{d}{dr}(\dot{m}\epsilon_i) = 0 \tag{1}$$

$$r^2 \rho D \frac{dY_i}{dr} + \dot{m}(\epsilon_i - Y_i) = 0 \tag{2}$$

$$\frac{d}{dr}\left[\dot{m} \Sigma h_i \epsilon_i - \lambda r^2 \frac{dt}{dr}\right] = 0 \tag{3}$$

$$\Sigma \epsilon_i = 1 \tag{4}$$

As a first approximation, a constant property solution was considered in the present analysis. Variable properties have been considered by others for steady burning at the wet bulb state.[4] However, in the heat-up period, this type of analysis becomes quite awkward. The constant property assumption decouples the mass and energy conservation equations, allowing an independent solution for species concentrations and temperatures. The constant
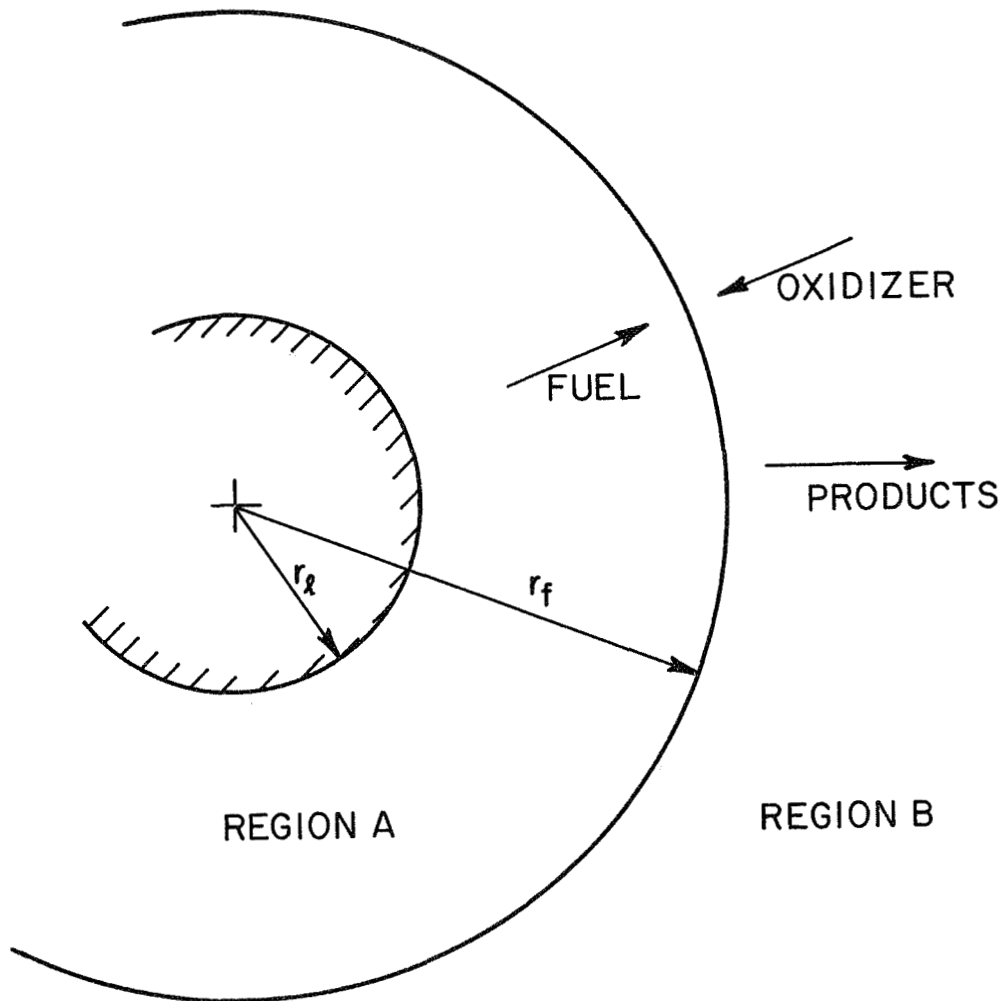
Fig. 2   Sketch of the Gas Phase Model.

and variable property solutions will be compared later for the case of steady burning at the wet bulb state.

In the following, each region is considered separately, with constant values employed for ρD, λ, and C_p in each region.

For conservation of mass in region A, the further assumption is made that the product species is insoluble in the liquid phase. Combining the insolubility assumption with the flame surface approximation yields the following boundary conditions for region A.

$$r = r_\ell \qquad Y_F = Y_{F\ell} , \qquad \varepsilon_F = 1$$

$$r = r_f \qquad Y_F = 0 \qquad\qquad\qquad (5)$$

With this set of boundary conditions, it is assumed that the droplet surface temperature is known so that the surface mole fraction of fuel can be determined from the Clausius Clapeyron equation and the total pressure. During the computation of a droplet life history, the droplet temperature is always known.

Equation (1) combined with the boundary condition for ε_F given in Eq. (5) yields $\varepsilon_F = 1$ throughout region A. Therefore, for the fuel, Eq. (2) takes the following form

$$r^2 (\rho D)_A \frac{dY_F}{dr} + \overset{\circ}{m} (1 - Y_F) = 0 \qquad\qquad (6)$$

Integrating Eq. (6) and applying the remaining two boundary conditions of Eq. (5) yields the following expression for the mass flux of fuel at the droplet surface.

$$\frac{\overset{\circ}{m}}{r_\ell (\rho D)_A} = \frac{-\ln (1 - Y_{F\ell})}{(1 - r_\ell / r_f)} \qquad\qquad (7)$$

The mass flux fractions of oxidizer and product in region B may be determined by assuming that the fuel and oxidizer combine in stoichiometric proportions at the flame surface as follows.

1 lbm fuel + i lbm oxidant $\rightarrow$ (1 + i) lbm prod.
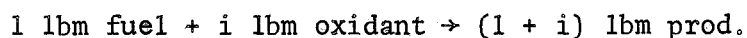
Noting that the mass flux fractions are constant in region B and that the oxidizer is diffusing towards the center of the droplet gives $\epsilon_x = -i$ and $\epsilon_p = 1 + i$ in region B. Thus for the oxidizer, Eq. (2) becomes

$$r^2 (\rho D)_B \frac{dY_x}{dr} - \dot{m} (i + Y_x) = 0 \tag{8}$$

subject to the following boundary conditions

$$r = r_f \qquad Y_x = 0 \qquad r = r_\infty \qquad Y_x = Y_{x_\infty} \tag{9}$$

Integrating Eq. (8) and introducing the boundary conditions from Eq. (9), yields the following expression for the mass flux.

$$\frac{\dot{m}}{r_f (\rho D)_B} = \ln (1 + Y_{x_\infty}/i) \tag{10}$$

Eliminating r_f between Eqs. (7) and (10) finally yields an expression for the total fuel mass flux at the droplet surface in terms of the known boundary conditions as follows:

$$\frac{\dot{m}}{r_\ell (\rho D)_A} = \ln \left\{ \frac{(1 + Y_{x_\infty}/i)^\phi}{(1 - Y_{F\ell})} \right\} \tag{11}$$

where

$$\phi = (\rho D)_B / (\rho D)_A \tag{12}$$

For the solution of the energy equation, the additional assumption is made that the specific heats of the product gas and the oxidizer are identical. Due to similar molecular weights, this assumption is reasonable in most cases. With the assumption of constant specific heats and the known mass flux fractions, Eq. (3) takes the following form in region A ($Cp_A = Cp_F$)

$$\frac{d}{dr} \left[\dot{m} Cp_A T - \lambda_A r^2 \frac{dt}{dr} \right] = 0 \tag{13}$$

with an analagous equation for region B ($Cp_B = Cp_x$). The boundary conditions on these equations are:

$$r = r_\ell, \quad T = T_\ell; \quad r = r_f, \quad T = T_f; \quad r = \infty, \quad T = T_\infty \qquad (14)$$

Integrating Eqs. (13), subject to the boundary conditions of Eqs. (14), yields the temperature distribution in each region. In reqion A

$$\frac{T - T_\ell}{T_f - T_\ell} = \frac{\exp\left\{\frac{\dot{m}\, Cp_A}{r_\ell\, \lambda_A}\left(1 - \frac{r_\ell}{r}\right)\right\} - 1}{\exp\left\{\frac{\dot{m}\, Cp_A}{r_\ell\, \lambda_A}\left(1 - \frac{r_\ell}{r_f}\right)\right\} - 1} \qquad (15)$$

and in region B

$$\frac{T - T_\infty}{T_f - T_\infty} = \frac{\exp\left\{\frac{-\dot{m}\, Cp_B}{r\, \lambda_B}\right\} - 1}{\exp\left\{\frac{-\dot{m}\, Cp_B}{r_f\, \lambda_B}\right\} - 1} \qquad (16)$$

Continuity of the energy flux at the flame surface provides a boundary condition that determines T_f. This relation is

$$\dot{m}\, Cp_F\, (T - T_0) + \dot{m}\, h_F^{\,\circ} - \lambda_A\, r^2\, \frac{dT}{dr}\,)_{f_A} =$$

$$\dot{m}\, Cp_B\, (T - T_0) + \dot{m}\, [\,(1 + i)\, h_p^{\,\circ} - h_x^{\,\circ}\,] - \lambda_B\, r^2\, \frac{dT}{dr}\,)_{f_B} \qquad (17)$$

where T_0 is a reference temperature for the evaluation of the enthalpy of formation, $h_i^{\,\circ}$. In the following, T_0 is taken to be T_ℓ for convenience. Evaluating the derivatives of Eqs. (15) and (16) and substituting into Eq. (17) gives the following

$$\frac{T_f - T_\ell}{T_\infty - T_\ell} = \frac{(1 + Q_R)\,(1 + Yx_\infty/i)^{-1/L_B} - Q_R}{1 - Cp_R\left[\dfrac{1 - (1 + Yx_\infty/i)^{-1/L_B}}{1 - (1 - Y_{F\ell})^{-1/L_A}}\right]} \qquad (18)$$

where

$$Cp_R = Cp_A / Cp_B \qquad (19)$$

$$L_{A,B} = \left(\frac{\lambda}{\rho Cp D} \right)_{A,B} \qquad (20)$$

and

$$Q_R = \frac{(1 + i) h_p^{\,\circ} - i h_x^{\,\circ} - h_F^{\,\circ}}{Cp_B (T_\infty - T_\ell)} \qquad (21)$$

Defining the droplet heat transfer coefficient as follows,

$$h = \frac{\lambda_A \frac{dT}{dr})_\ell}{(T_\infty - T_\ell)} \qquad (22)$$

the Nusselt number becomes

$$\frac{h d_\ell}{\lambda_A} = \frac{2}{L_A} \left(\frac{T_f - T_\ell}{T_\infty - T_\ell} \right) \ln \left\{ \frac{(1 + Y x_\infty / i)^\phi}{(1 - Y_{F\ell})} \right\} \bigg/ \left[(1 - Y_{F\ell})^{-1/L_A} - 1 \right] . \qquad (23)$$

Transport rates at the droplet surface may be found if the instantaneous temperature of the liquid surface, the ambient temperature and the ambient oxidant concentration are known. The vapor pressure curve of the fuel gives $Y_{F\ell}$ from T_ℓ and Eq. (18) can then be employed to determine T_f. In this procedure, average properties can be determined by iteration from the computed flame temperature. Once the flame temperature and average properties are specified, Eqs. (11) and (23) give the instantaneous heat and mass transfer rates at the droplet surface.

Some of the general characteristics of this solution may be seen by considering the simplified case where $\phi = Cp_R = L_A = L_B = 1$. This corresponds to a unity Lewis number solution with identical properties both inside and outside the combustion zone. For this situation, Eqs. (11), (18) and (23) become:

$$\frac{\dot{m}}{r_\ell \rho D} = \ln \left\{ \frac{1 + Y x_\infty / i}{1 - Y_{F\ell}} \right\} \qquad (24)$$

$$\frac{T_f - T_\ell}{T_\infty - T_\ell} = \frac{Y_{F\ell}\,(1 - Q_R\,Yx_\infty/i)}{(Y_{F\ell} + Yx_\infty/i)} \qquad (25)$$

$$\frac{hd\ell}{\lambda} = 2\,\frac{\dot{m}}{r_\ell \rho D}\,\frac{(1 - Y_{F\ell})\,(1 - Q_R\,Yx_\infty/i)}{(Y_{F\ell} + Yx_\infty/i)} \qquad (26)$$

For hydrocarbon oxidation the parameter Yx_∞/i typically varies in the range $0 - .4$ as the ambient gas varies from decomposition conditions to pure oxygen. Equation (24) is illustrated in Figure 3 for this range of Yx_∞/i and various values of $Y_{F\ell}$. The mass transfer rate increases rapidly with increasing $Y_{F\ell}$. For finite values of Yx_∞/i, the mass transfer does not go to zero for $Y_{F\ell} = 0$. In this formulation, fuel is consumed at the droplet surface, through the requirement of stoichiometric combination of fuel and oxidizer at the flame, and the total fuel consumption is determined by the oxidizer diffusion rate to the droplet surface. Thus, at low values of $Y_{F\ell}$, the mass transfer rate is influenced quite strongly by the ambient oxygen concentration.

At values of $Y_{F\ell}$ approaching unity, the combustion zone moves far from the droplet and the mass transfer rate is less sensitive to its actual position. At this condition, the mass transfer rate is only weakly influenced by the ambient oxygen concentration for a given $Y_{F\ell}$.

The Nusselt number is plotted in Fig. 4 as a function of $Y_{F\ell}$ for the same range of Yx_∞/i as in Fig. 3. In all cases, the Nusselt number decreases with increasing $Y_{F\ell}$ due to the increased amount of energy swept back into the ambient fluid by the greater radial mass flux at high $Y_{F\ell}$.

For finite Yx_∞, the Nusselt number depends on the value of Q_R. Two values of Q_R are examined in FIg. 4. The value, $Q_R = 1$, represents a relatively high ambient temperature as in the present experiment or in a rocket engine combustion chamber. The second value, $Q_R = 10$, would be typical of
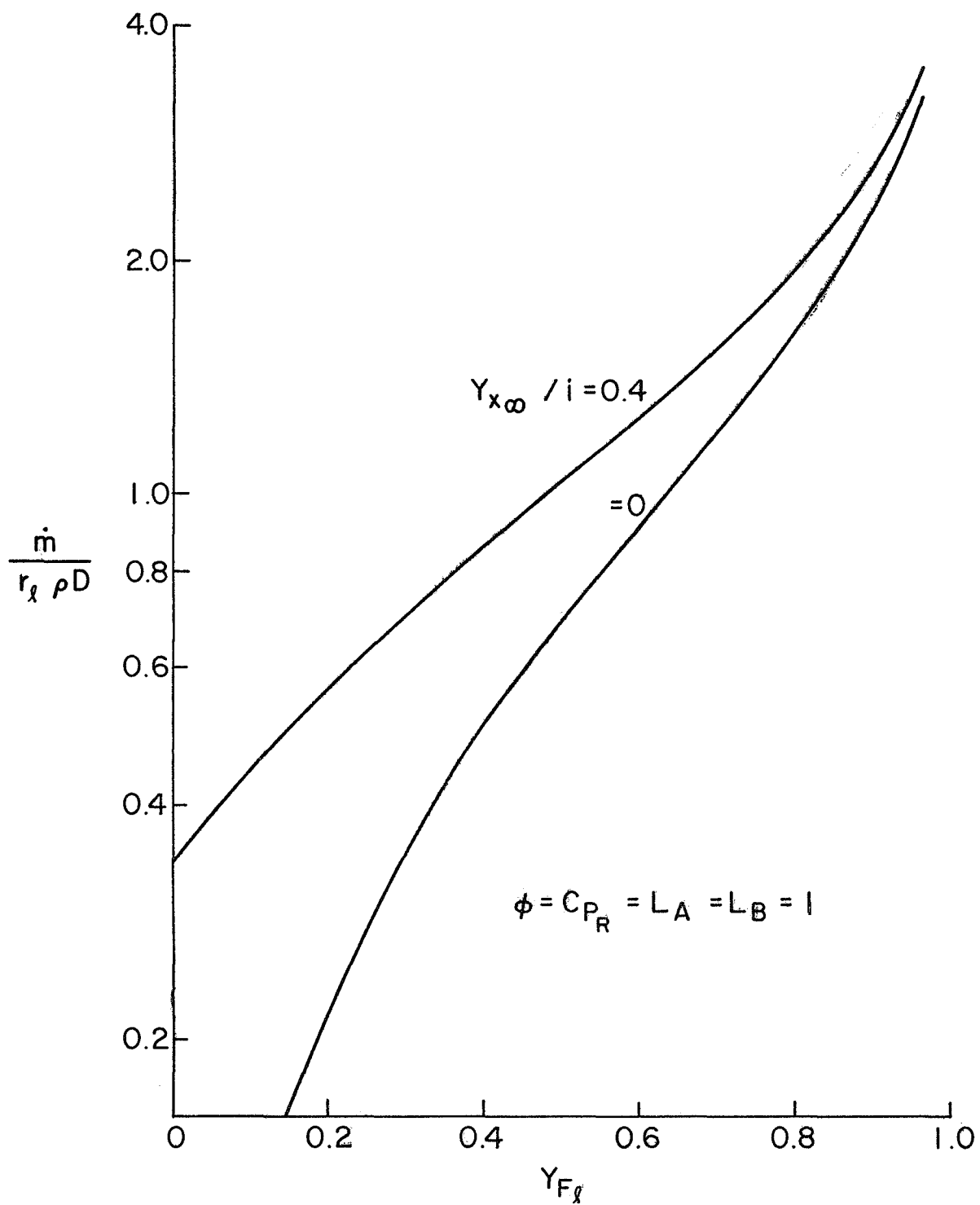
Fig. 3 Mass Transfer Rate as a Function of $Y_{F\ell}$.
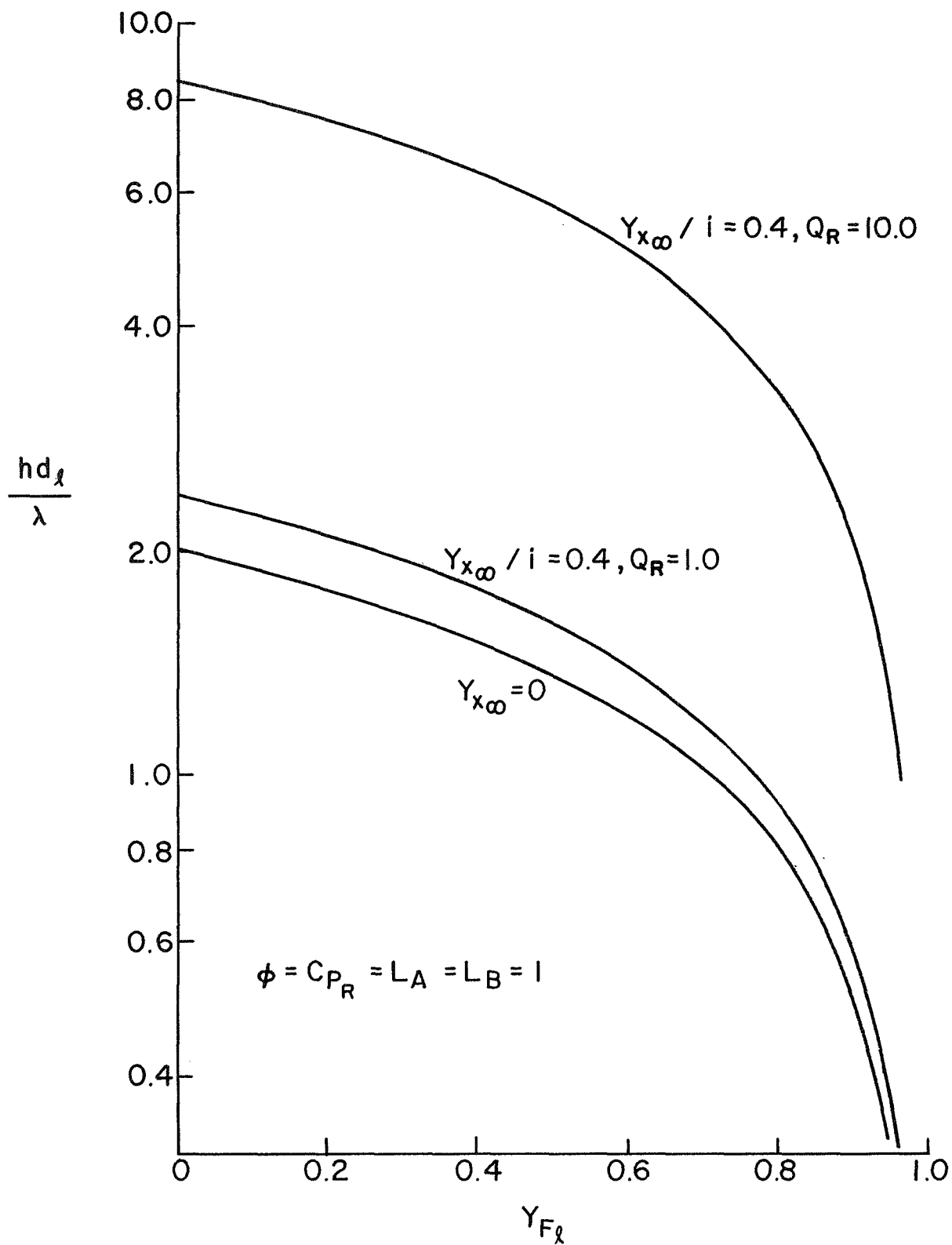
Fig. 4   Nusselt Number as a Function of Y_{Fl}.

droplets burning in a moderately heated environment as in the experiments of Ref. 3, 9, 14. For low values of Q_R, the ambient oxygen concentration exerts only a small influence since the ambient temperature is near the flame temperature.

The heat and mass transfer equations may be combined to yield an expression for the steady burning rate of a droplet at its wet bulb temperature.[1-6] This aspect of the solution will be examined later along with the experimental results. In their present form, the transport equations are valid at any point in the life history of a droplet.

Convection Correction: The analysis presented in the previous section is limited to the case of no relative motion between the droplet and its surroundings. For the present tests, however, the flow of the product gas past the droplet gave Reynolds numbers (based on approach conditions) in the range 1 - 10. Therefore, the theory must be corrected for the influence of forced convection, if comparison is to be made with the present experimental results.

For steady droplet evaporation or burning at the wet bulb state, numerous investigators have suggested a convection correlation of the following form

$$\frac{\dot{m}}{\dot{m}^*} = 1 + f \ (Re, \ Pr, \ Sc) \tag{27}$$

where $\dot{m}^*$ is the evaporation rate at no flow.[13-18] For incipient convection, constant properties and chemical reaction limited to a flame surface, Fendel, et al, have demonstrated the validity of this general form with some rigor.[16,17] For larger Reynolds numbers, there is no theoretical justification for Eq. (27), but this type of correlation appears to be satisfactory within the accuracy of the data currently available in the literature.[18]

An identical equation is also appropriate for heat and mass transfer taken independently.[19-21] Therefore, it is proppsed to correct Eqs. (11) and (23) by a relation of the form of Eq. (27).

While there is general agreement that transport quantities can be corrected for convection with an equation of the form of Eq. (27), there is less agreement concerning the details of the correlation. Unfortunately, the disagreement is greatest for Reynolds numbers less than ten, which is the range of interest in the present investigation.

For low values of Peclet number (pe = RePr) Fendell, et al,[16,17] and Acrivos and Taylor[21] have found the following equation through rigorous application of the method of inner and outer expansions.

$$\left(\frac{\dot{m}}{\dot{m}^*} \text{ or } \frac{Nu}{Nu^*} \right) = 1 + \frac{1}{4} RePr + 0 \ (Pe^2 \ln Pe) \qquad (28)$$

For higher Reynolds numbers, mostly Re > 10, a number of empirical correlations have been presented, of the form

$$\left(\frac{\dot{m}}{\dot{m}^*} \text{ or } \frac{Nu}{Nu^*} \right) = 1 + C \ Re^{1/2} \ Pr^{1/3} \qquad (29)$$

where the constant C has varied with the investigator. For example, Frössling[15] finds C = .276 while Ranz and Marshall[19] find C = .300. The Schmidt number replaces the Prandtl number when the correlation is applied to mass transfer alone. However, Eq. (29) has been used for burning droplets since the Prandtl number can be evaluated less ambiguously.[13] Since the Prandtl and Schmidt numbers are approximately the same for most gases, this substitution presents little difficulty in practice.

While Ranz and Marshall[19] claim that Eq. (29) is valid for low Reynolds numbers, this question does not reduce to the rigorous form, Eq. (28), for Pe << 1. In a more recent experiment, Yuge[20] carefully accounted for the influence of natural convection at low Reynolds numbers. His data agrees with the Frössling correlation (and also with Allender's data[22]) for Re > 10. For Re < 10, the Yuge data falls below the Frössling correlation.

Prompted by this difficulty in the convection correlation for Reynolds numbers of order unity, Fendell, et al[17] and Rosner[18] have suggested some general forms that are asymptotically correct for Pe << 1 and Re > 10. Adopting the form suggested by Rosner,[13] and fitting the correlation to the data of Yuge,[20] and Frössling,[15] and Allender[22] at Re = 100, Pr = .715, yields the following expression

$$\left(\frac{\dot{m}}{\dot{m}^*} \quad \text{or} \quad \frac{Nu}{Nu^*} \right) = 1 + .278 \ Re^{1/2} \ Pr^{1/3} \ [1 + 1.237 \ Re^{-1} \ Pr^{-4/3}]^{-1/2} . \quad (30)$$

Equation (30), asymptotically approaches Eq. (28) for RePr << 1. The equation is also in good agreement with Yuge's low Reynolds number data in the range 3.5 < Re < 10, as well as the results of Refs. 15, 20, and 22 for 10 < Re < 800.

Equation (30) was employed in the present investigation. According to criterion developed by Yuge,[20] and necessarily applied rather crudely for the present reactive case, natural convection can be neglected in the present experiments.

Liquid Phase Analysis: For the treatment of the liquid phase, the droplet temperature was assumed to be uniform at each instant of time. Temperature gradients within the droplet have been considered by a number of authors.[23-25] In general, this effect has only a small influence on droplet lifetimes and steady burning rates at atmospheric pressure.

With the assumption of a uniform droplet temperature, and neglecting the time derivatives of liquid properties, the equations of conservation of mass and energy of the droplet become

$$\frac{d}{dt} \ (m) = -4 \ \pi \ \dot{m} \quad (31)$$

$$\frac{dT_\ell}{dt} = \frac{4\pi}{mCp_\ell} \ (\dot{q} - h_{fg} \ \dot{m}) \quad (32)$$

where $\dot{q}$ is the energy flux reaching the droplet per unit solid angle

$$\dot{q} = r_\ell^2 \, h \, (T_\infty - T_\ell) \qquad\qquad (33)$$

The diameter of the droplet is related to its mass and density as follows,

$$d_\ell = \left(\frac{6m}{\pi \rho_\ell} \right)^{1/3} \qquad\qquad (34)$$

For a calculation of a droplet life history, the initial conditions become

$$t = 0; \quad T_\ell = T_{\ell 0}; \quad d_\ell = d_{\ell 0} \qquad\qquad (35)$$

From these initial conditions, the subsequent droplet temperature and diameter were computed by numerically integrating Eqs. (31) and (32). The quantities $\dot{m}$ and $\dot{q}$ were determined from Eqs. (11) and (23), and corrected for convection with Eq. (30).

Unless noted otherwise, gas phase properties were computed for the average composition and log mean average temperature in each region. The log mean temperature was determined iteratively from the computation of the flame temperature, Eq. (18). Liquid phase properties were calculated at the instantaneous liquid temperature, T_ℓ. For the bulk of the calculations, properties in the convection correction equation, Eq. (30), were taken to be those of the ambient gas, as suggested by Combs.[26] A second method for selecting properties in this correction suggested by Eisenklam, et al,[14] was also attempted. A comparison of these two approaches will be made later. The specific property correlations utilized for all the properties are presented in Appendix A.

Much of the data obtained in the present investigation involved measurements of the steady droplet burning rate, at the wet bulb state of

the droplet. At this condition, $dT_\ell/dt = 0$ by definition and Eq. (32) can be solved to yield the following expression for $Y_{F\ell}$.

$$Y_{F\ell} = 1 - \left[1 + \frac{Cp_A (T_f - T_\ell)}{h_{fg}}\right]^{-L_A} \tag{36}$$

Substitution of Eq. (36) into Eq. (18) then yields

$$\frac{T_f - T_\ell}{T_\infty - T_\ell} = \frac{[Cp_B (T_\infty - T_\ell) + H_c + h_{fg}] (1 + Yx\infty/i)^{-1/L_B} - H_c - h_{fg}}{Cp (T_\infty - T_\ell)} \tag{37}$$

A convenient way of reducing steady burning data involves the use of the burning rate constant.[2,4] This parameter is defined as follows

$$K = - \frac{dd_\ell^2}{dt} \tag{38}$$

In terms of the present theoretical model, the burning rate parameter becomes

$$K = \frac{8 (\rho D)_A}{\rho_\ell} \ln \left\{(1 + Y_{x\infty}/i)^\phi \left[1 + \frac{Cp_A (T_f - T_\ell)}{h_{fg}}\right]^{L_A}\right\} \frac{\dot{m}}{\dot{m}^*} \tag{39}$$

where $\frac{\dot{m}}{\dot{m}^*}$ is given by Eq. (30).

Equation (39) is dependent on d_ℓ, through the Reynolds number in Eq. (30). However, the dependence is not strong for the Reynolds number range considered in the present tests, and a plot of d_ℓ^2 vs time is approximately linear during steady burning.

BURNING RATE RESULTS

The burning rate constant, defined in Eq. (38), was obtained from the experimental variation of diameter squared with time. A typical diameter squared plot is given in Fig. 5. The slope was measured at a fixed average diameter of 1100μ in order to eliminate variations due to the influence of convection as discussed earlier. For the droplet sizes tested, this diameter was sufficiently removed from the heat-up period to provide a good estimation of the steady burning rate.

The burning rate constants reported here are average values obtained from four separate tests. Typically, the values from the individual tests were within 3% of the average.

Effect of Ambient Temperature: The first series of tests considered the influence of ambient temperature on high temperature droplet evaporation. For these tests, the ambient oxygen concentration was less than 1%, through dissociation. The ambient gas velocity was also maintained essentially constant at 46.7 cm/sec. The experimental results for methanol, n-pentane, and n-decane are given in Figs. 6, 7, and 8.

The theoretical curves on the figures were constructed for two different methods of selecting properties in the convection correction (Eq. 30) as well as results obtained by neglecting convection entirely (curve A). Curve B was computed by evaluating properties in Eq. (30) for conditions in the ambient gas, as suggested by Combs.[21] Curve C was computed with properties in the convection correction evaluated at mean conditions in the droplet boundary layer as suggested by Eisenklam, et al[14].

For the particular conditions of these tests, the different methods only change the levels and not the slopes of the curves. The percentage difference increases at the lower temperatures, however, due to the increased Reynolds number for a fixed gas velocity.
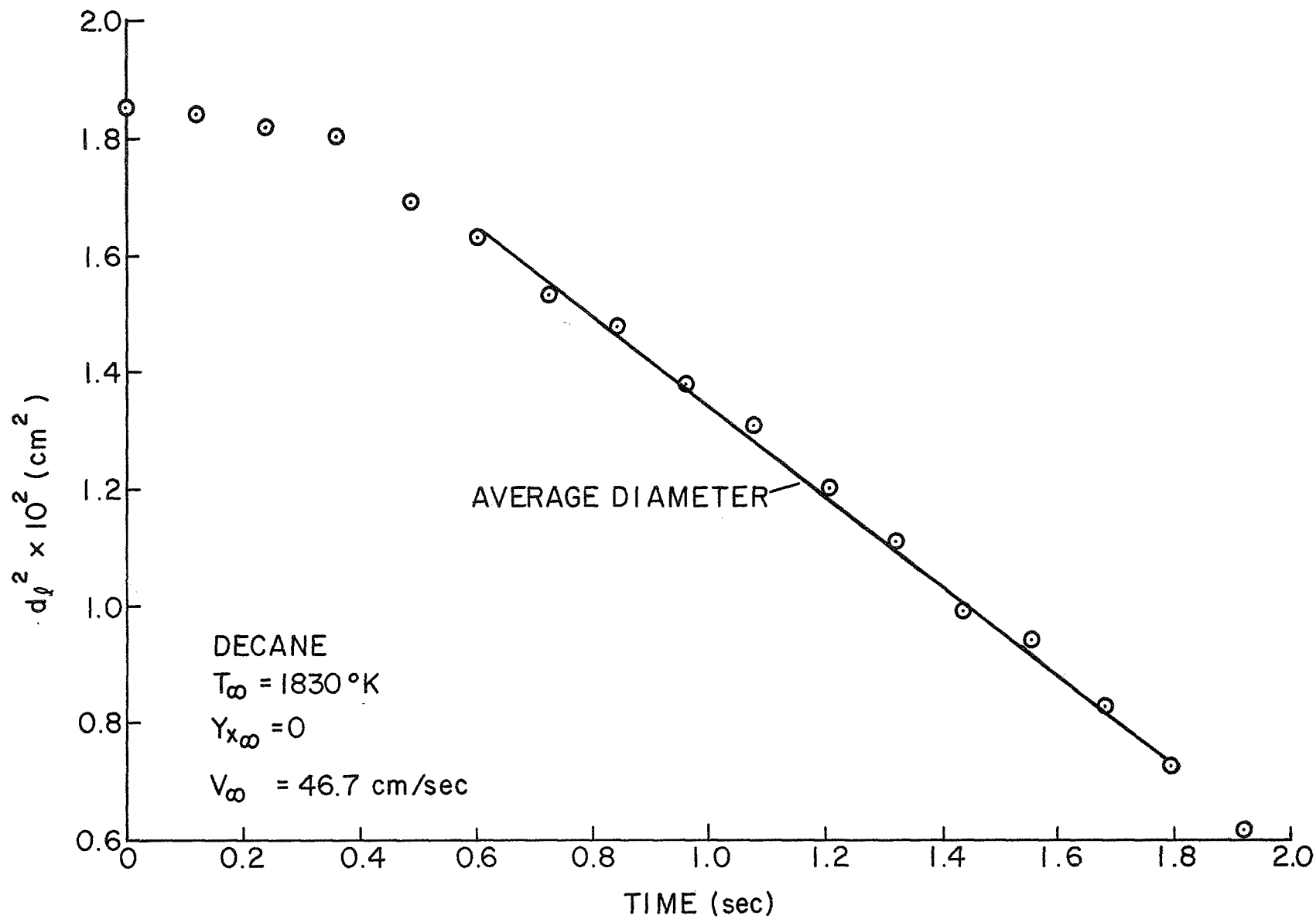
Fig. 5   A Typical Diameter Squared Plot.
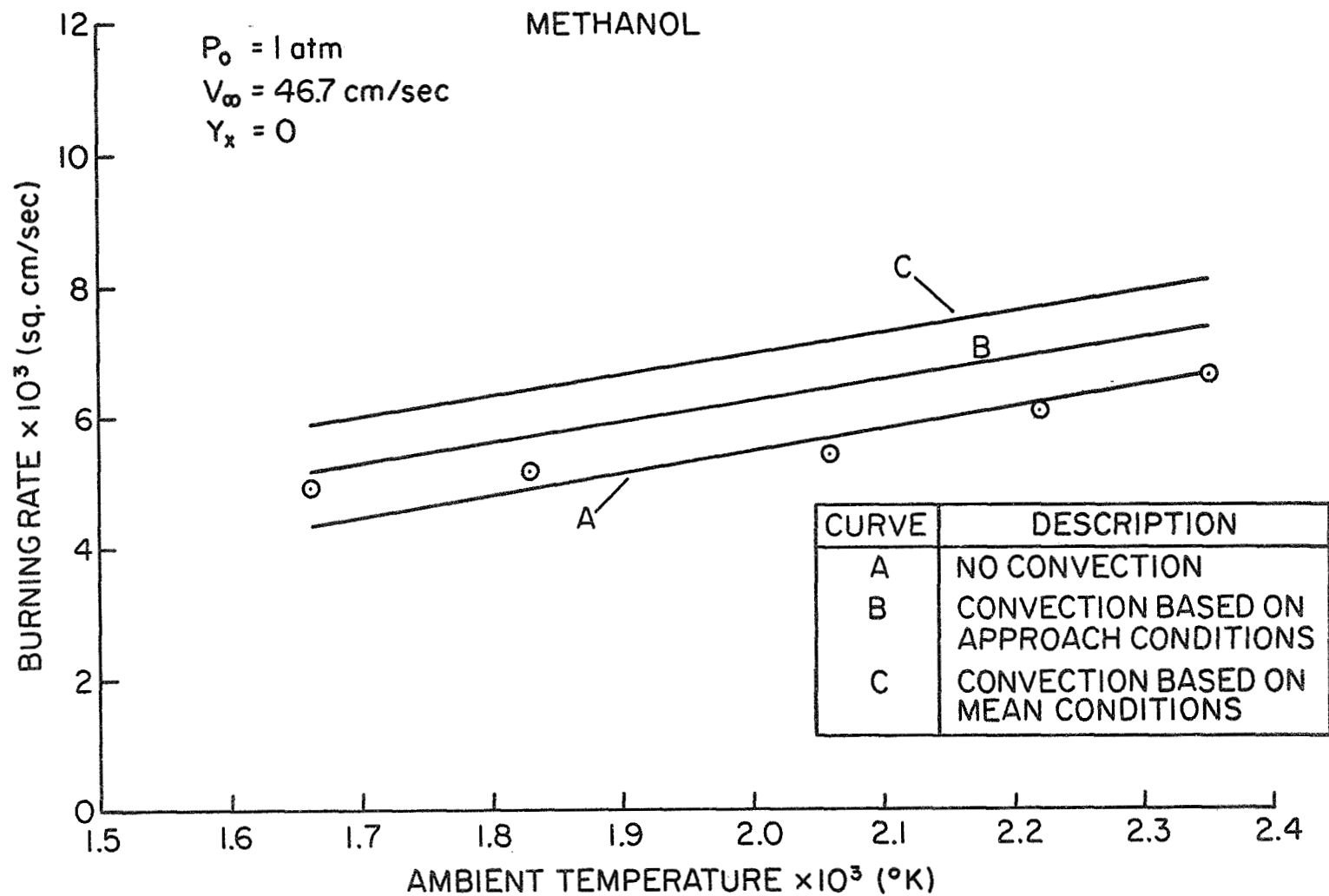
Fig. 6   Methanol Evaporation at Various Ambient Temperatures, d_ℓ avg = 1100 μ.
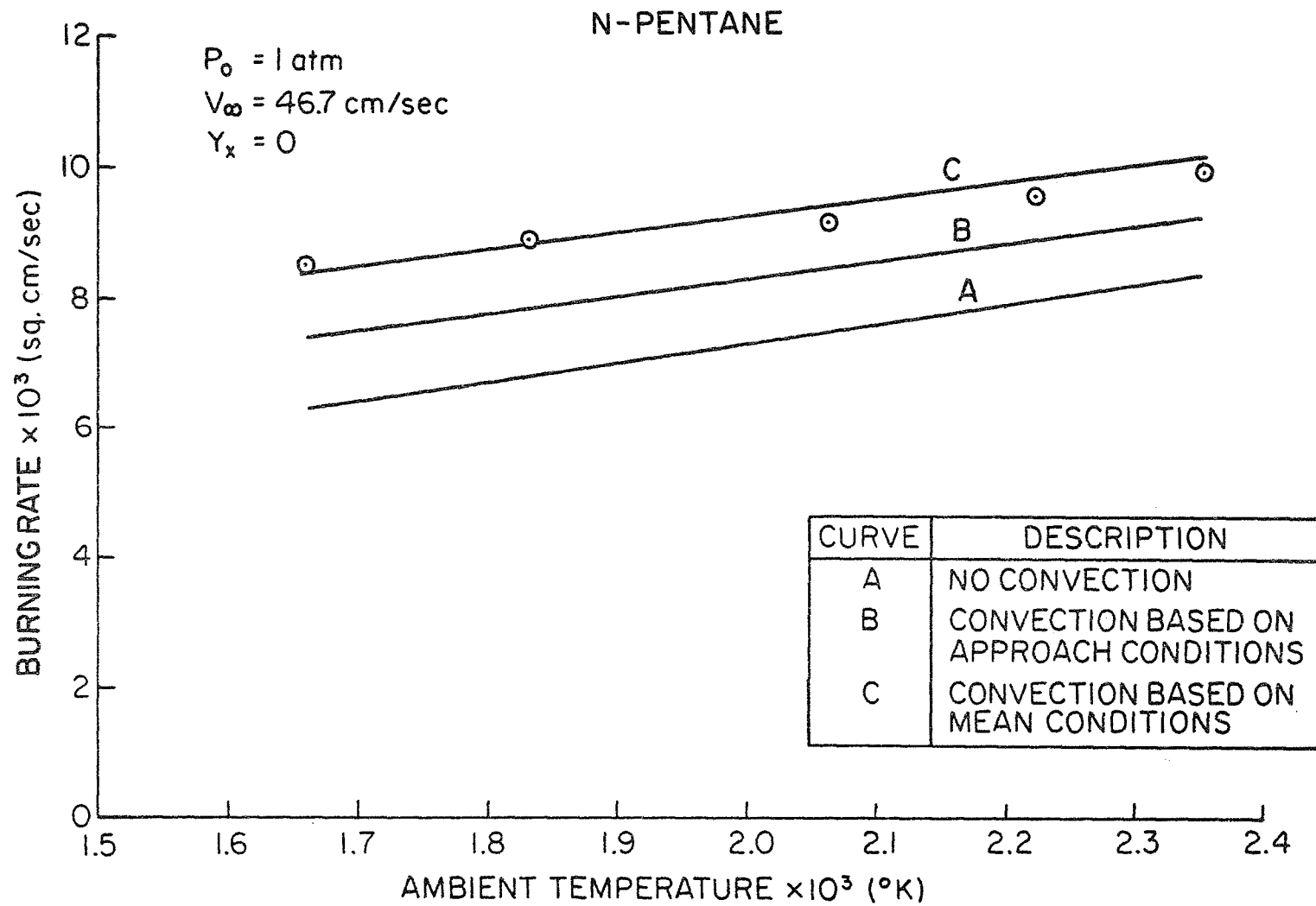
Fig. 7   n-Pentane Evaporation Rates at Various Ambient Temperatures, $d_\ell avg = 1100\mu$.
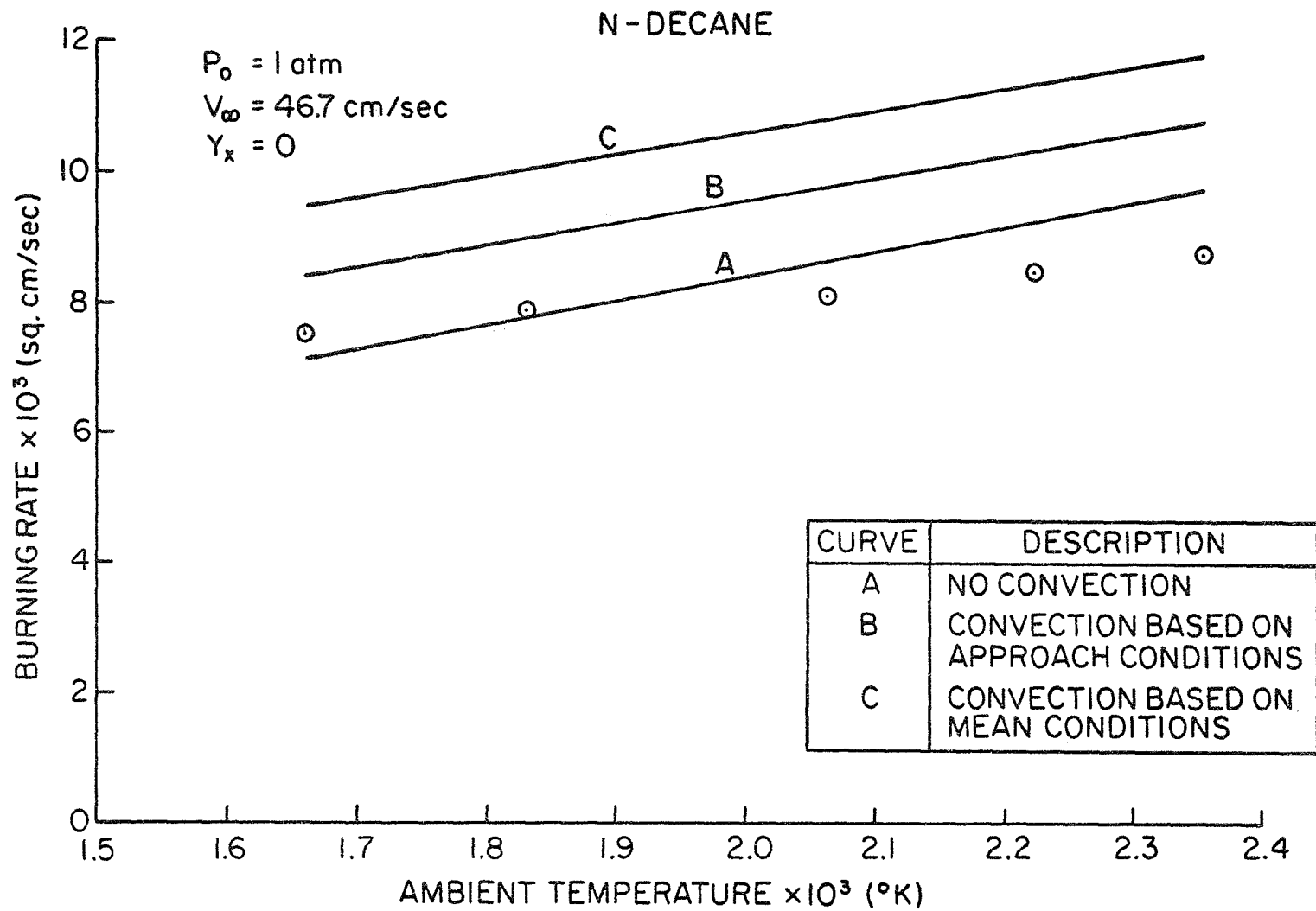
Fig. 8   n-Decane Evaporation Rates at Various Ambient Temperatures, d_ℓ avg = 1100μ.

Aside from the levels of the theoretical curves, which are influenced by the particular method chosen for selecting average properties, the trend of the theoretical prediction appears reasonably satisfactory for methanol and n-pentane. The predicted increase in the evaporation rate of n-decane with increasing temperature, somewhat overestimates the measured increase in evaporation rate.

The plots indicate that the influence of convection was not large for these test conditions. Therefore, it is not possible to make a clear choice between methods B and C for correlating convection effects. In the following, method B is employed, since the large property differences in regions A and B causes difficulties in selecting unambiguous mean properties for use in method C. Furthermore, as will be discussed later, method B appears to give a more satisfactory prediction of the variation in burning rate due to changes in fuel molecular weight.

Effect of Ambient Oxygen Concentration: Figures 9, 10, and 11 show the results of burning rate measurements for methanol, n-pentane and n-decane at various ambient oxygen concentrations. The oxygen mass fraction on the plots is an effective mass fraction based on the ambient concentration of possible oxidizing species (O_2, O and NO). In these tests, the ambient gas temperature and velocity were maintained essentially constant at 2530°K and 62.5 cm/sec respectively.

Two simplified theoretical approaches were taken with regard to the chemical energy release in the reaction zone. In the first approach, dissociation was neglected and the standard heat of reaction was employed in the calculations. Partial correction of the effect of dissociation in the reaction zone was made in the second method through the use of a corrected heat of reaction. The corrected heat of reaction was taken as the actual
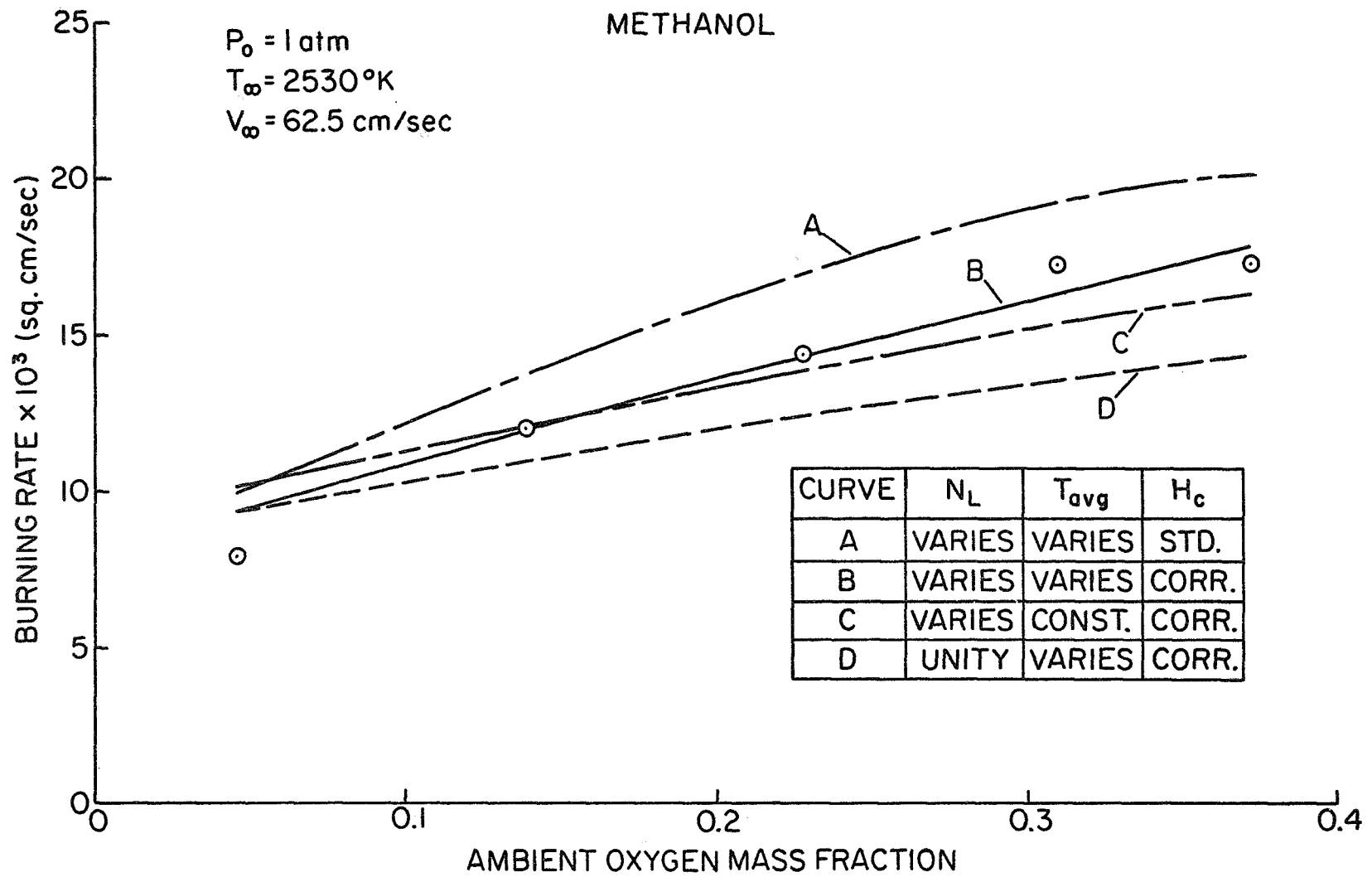
Fig. 9   Methanol Evaporation Rates at Various Ambient Oxygen Concentrations, $d_\ell avg = 1100\mu$.
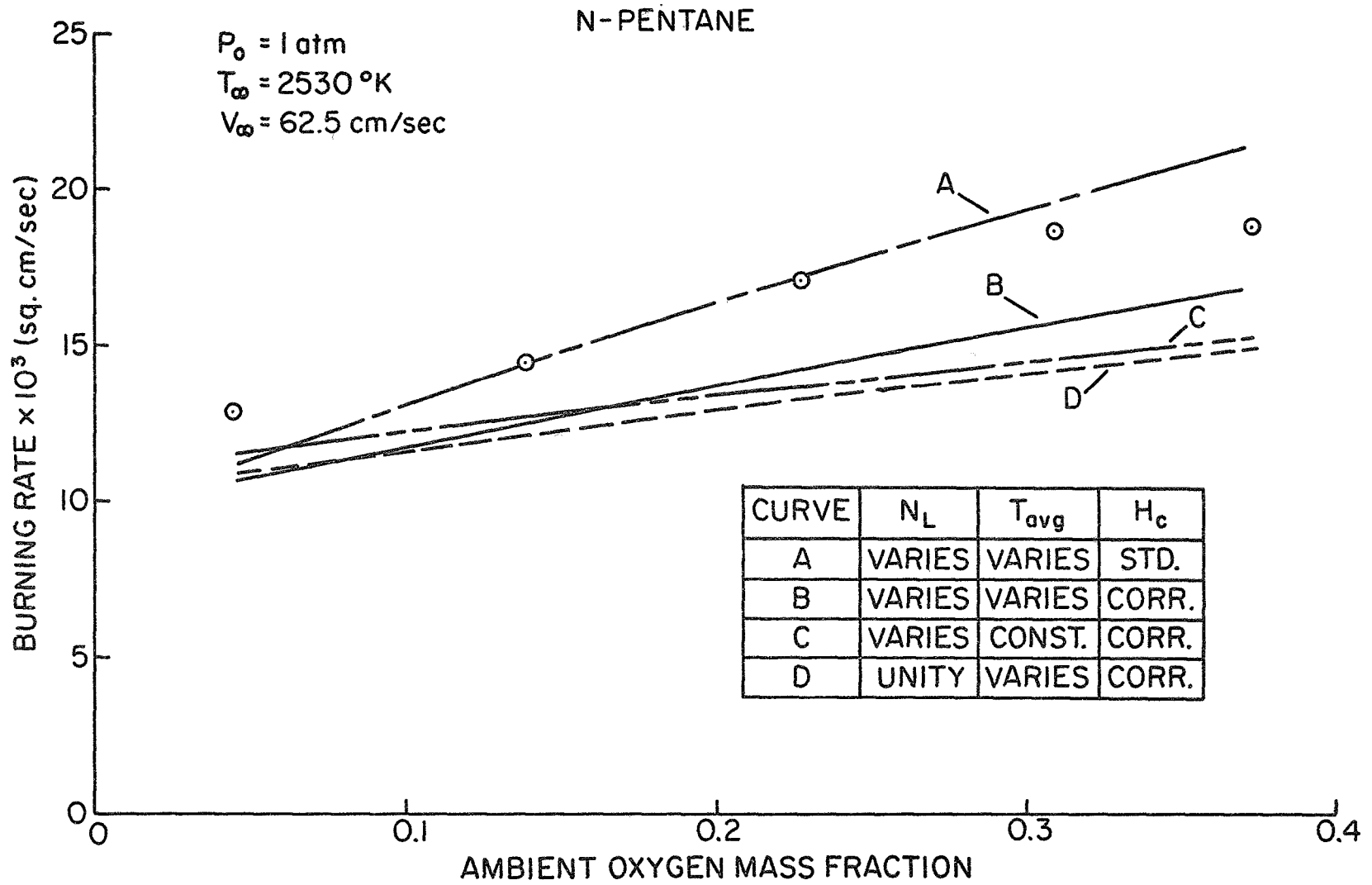
N-PENTANE

$P_0 = 1$ atm
$T_\infty = 2530\,°K$
$V_\infty = 62.5$ cm/sec

CURVE	N_L	T_{avg}	H_c
A	VARIES	VARIES	STD.
B	VARIES	VARIES	CORR.
C	VARIES	CONST.	CORR.
D	UNITY	VARIES	CORR.

Fig. 10   n-Pentane Evaporation Rates at Various Ambient Oxygen Concentrations, $d_\ell$avg = 1100μ.

N-DECANE

$P_o = 1$ atm
$T_\infty = 2530 °K$
$V_\infty = 62.5$ cm/sec

A

B

C

D

CURVE	N_L	T_{avg}	H_c
A	VARIES	VARIES	STD.
B	VARIES	VARIES	CORR.
C	VARIES	CONST.	CORR.
D	UNITY	VARIES	CORR.

BURNING RATE $\times 10^3$ (sq. cm/sec)

AMBIENT OXYGEN MASS FRACTION
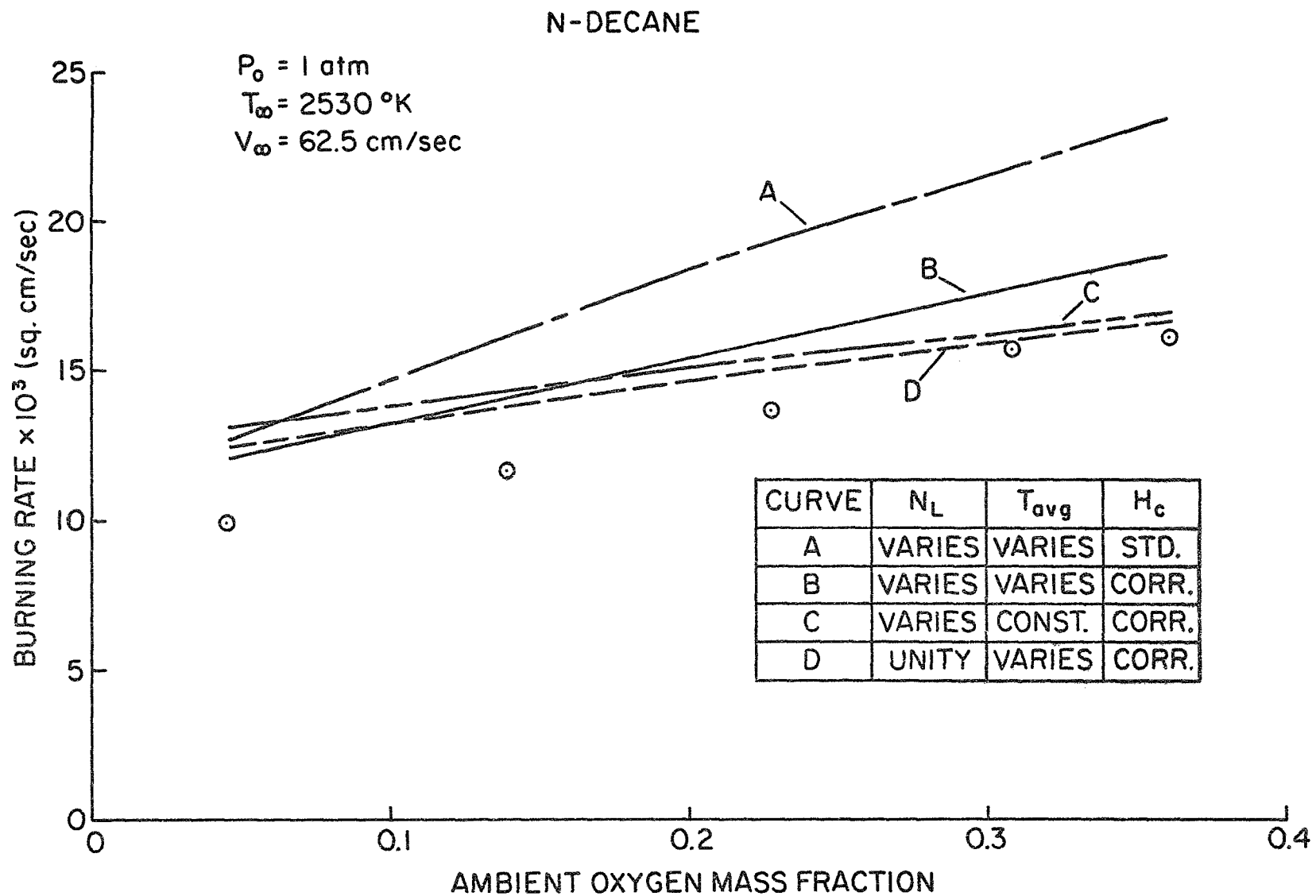
Fig. 11   n-Decane Evaporation Rates at Various Ambient Oxygen Concentrations, $d_\ell$avg = 1100μ.

chemical energy release, allowing for dissociation, for stoichiometric adiabatic combustion. The numerical values employed in the calcualtions are given in the Appendix.

Computed droplet flame temperatures for these two energy release models are shown in Table II. The corrected values are more realistic in view of dissociation effects, but are probably still too high for the higher oxygen concentrations.

Computed burning rate constants for these two methods, as well as several other modifications of the theory, are compared with the data in Figs. 9, 10, and 11. Curve A was constructed for a non-unity Lewis number and a standard heat of reaction, with properties computed at the log mean temperature in both regions. The log mean temperature was determined iteratively from the computed flame temperature.

Method B is similar to method A except that the corrected heat of reaction was employed in the calculations. Method C is similar to method B with the exception that gas properties were not varied with the oxygen concentration (in response to the changing flame temperature). Method D is also similar to method B except that the diffusion coefficients were chosen to give unity Lewis number throughout the flow field. Methods C and D were considered since a number of investigators have used these approaches.[1-3,6]

The figures indicate that there are only small differences between methods B, C, and D, although method B appears to give a slightly superior representation of the trends of the data. Methods A and B are identical at zero ambient oxygen concentration, with differences increasing up to 20% at the maximum ambient oxygen concentration of these tests.

The various approaches for selecting properties in the theory were examined further by considering some burning rate data for decane at low

TABLE II: COMPUTED FLAME TEMPERATURES DURING STEADY BURNING

FUEL	THEORY	FLAME TEMPERATURE ($^\circ$K)		
		$Y_x = 0.0455$	$Y_x = 0.2269$	$Y_x = 0.3713$
METHANOL	STD H_c	2850	4040	4770
	CORRECTED H_c	2700	3330	3730
N-PENTANE	STD H_c	2800	4310	5370
	CORRECTED H_c	2650	3345	3850
N-DECANE	STD H_c	2790	4290	5370
	CORRECTED H_c	2645	3350	3860

ambient temperatures (297°K). This data was obtained in the zero-gravity apparatus described in Ref. 27, in order to eliminate uncertainties in the evaluation of the influence of natural convection.

The experimental results for these tests are compared with the theoretical methods in Fig. 12. Methods A and C show large errors in both the magnitude and trends of the data. Methods B and D give comparable results, with maximum errors of approximately 50%. The largest percentage of errors are obtained for the lower oxygen concentrations.

Effect of Molecular Weight: The results up to this point indicate an apparently random shifting of the theoretical curves above and below the experimental results for the different fuel types. This behavior was examined in a more systematic way by comparing the theory and measurements for a large range of fuel types. Figure 13 shows this comparison for normal paraffin fuels ranging from n-pentane to n-hexadecane. Figure 14 shows a similar comparison for 1-alcohols ranging from methanol to decyl alcohol. These tests were conducted for three different ambient oxygen concentrations while maintaining a constant ambient gas temperature and velocity of 2530°K and 62.4 cm/sec respectively.

Method B was employed to compute the theoretical results on Figs. 13 and 14. This method was selected since it showed the best overall agreement with the experimental data.

For both the alcohols and the paraffins, the trend of the theoretical curves with increasing molecular weight is not in good agreement with the experimental results. The theory increasingly overestimates the burning rate for the heavier hydrocarbons.

Use of the Eisenklam, et al[14] method for selecting properties in the convection correlation would only make the failure worse for the heavier hydrocarbons. In this method, increasing fuel molecular weight causes an
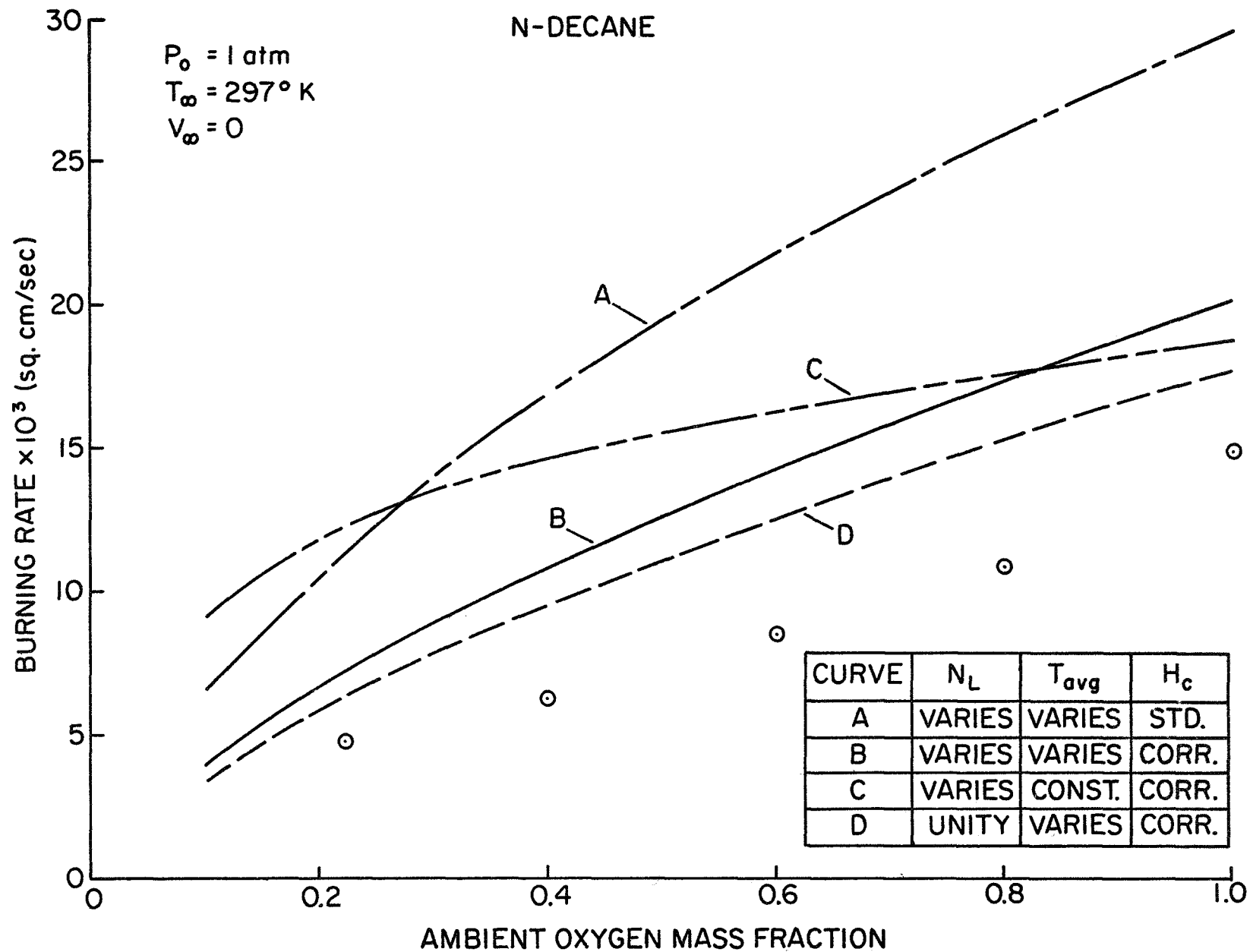
Fig. 12   Low Ambient Temperature Burning Rates for n-decane at Various
            Ambient Oxygen Concentrations Under Zero Gravity Conditions, $d_\ell avg$ =
            1100μ.

ALCOHOLS

$P_0 = 1$ atm
$T_\infty = 2530\,°K$
$V_\infty = 62.5$ cm/sec

$Y_x = 0.3713$, METHOD B

$Y_x = 0.2269$

$Y_x = 0.0455$

BURNING RATE $\times 10^3$ (sq. cm/sec)

SYMBOL	Y_x
⊙	0.0455
⊡	0.2269
△	0.3713

NUMBER OF CARBON ATOMS
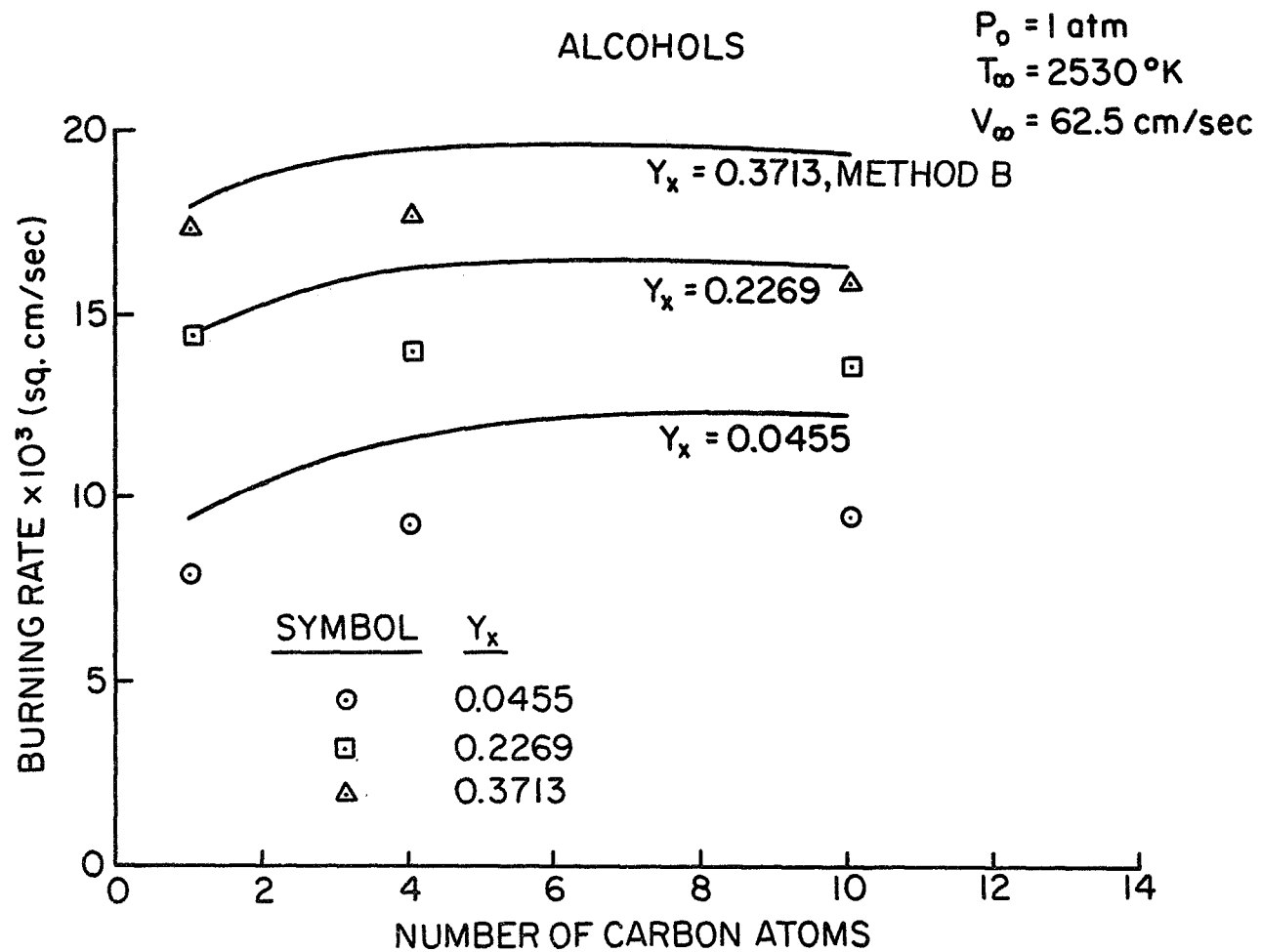
Fig. 13   Theoretical and Experimental Burning Rates for Various Alcohols,
$d_\ell$avg = 1100μ.

35
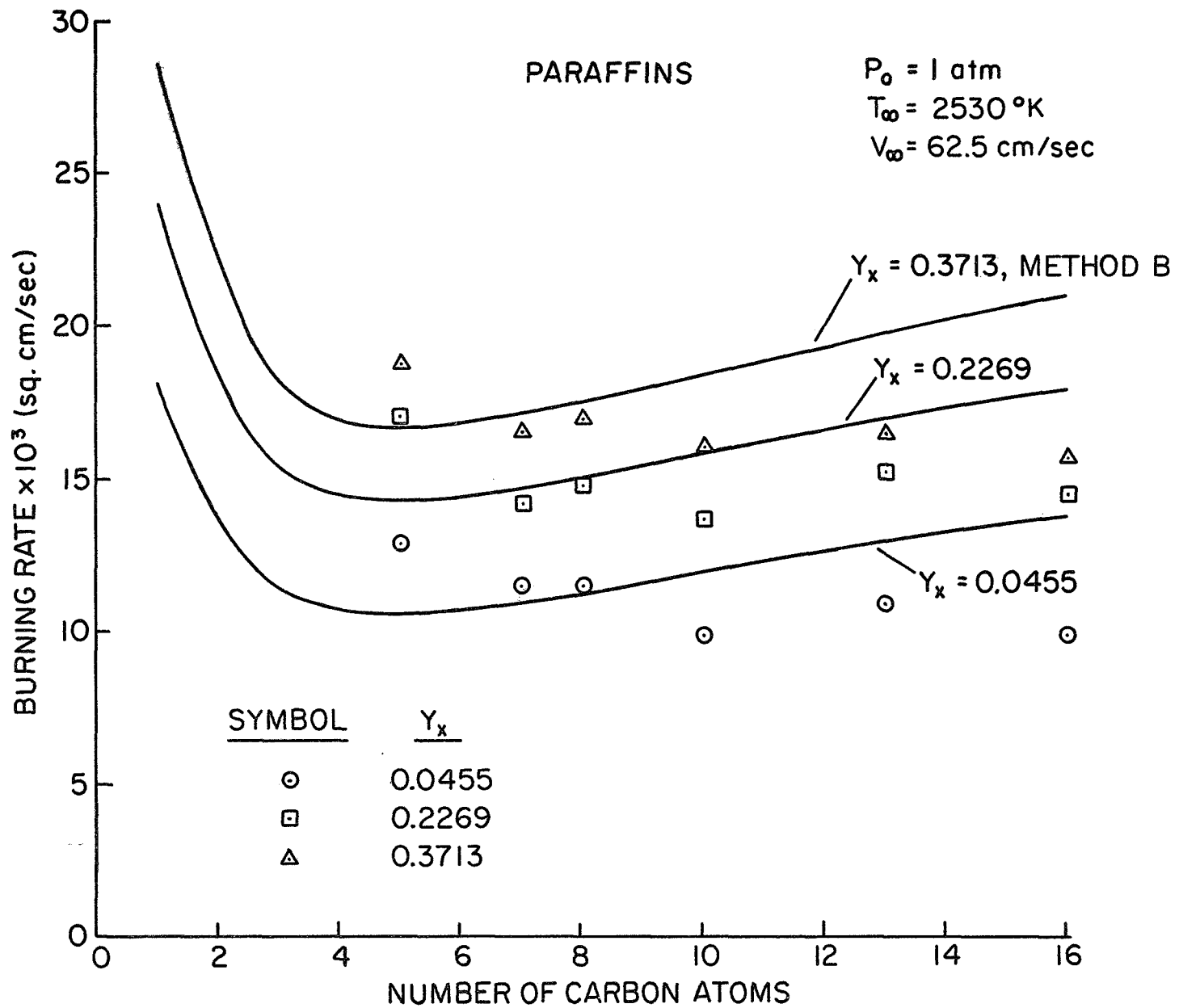
Fig. 14   Theoretical and Experimental Burning Rates for Various Paraffins, $d_\ell avg = 1100\mu$.

increase in the Reynolds number in Eq. (30), for fixed ambient conditions. This, in turn, increases the convection correction for the heavier molecular weight materials causing the theoretical curves to rise even faster than the curves shown in Figs. 13 and 14.

DISCUSSION OF BURNING RATE RESULTS

Method B gives the best representation of the trends of the data, and the least absolute error over the range of experimental results available for comparison in this study. Maximum errors were encountered for the low ambient temperature results for decane (70%). Restricting attention to the high ambient temperatures which are more representative of combustion chamber conditions, the maximum error over the test range was 38% (cetane at low ambient oxygen concentration). For lighter hydrocarbons the errors were smaller, e.g. 25% for all materials having less than ten carbon atoms. Fig. 15 shows a composite comparison of the theoretical (method B) and experimental burning rate constants over the entire test range.

Considering the uncertainties in physical properties, and the relative crudeness of the model, errors of this magnitude are perhaps reasonable. However, the systematic failure of the theory to give the correct trend with increasing fuel molecular weight, casts doubt on the ability of this model to provide a reliable framework for combustion chamber calculations, where operating pressures and droplet diameters are markedly different from those employed in the present investigation.

The data of Hottel, et al,[3] also exhibits this type of failure with respect to molecular weight for somewhat heavier paraffin hydrocarbons than those considered in the present investigation. Some theoretical and experimental results of Ref. 3 are given in Table III. While both the details of the theory and the experiment of Ref. 3 are different from the present investigation, the trends are qualitatively the same. The prediction indicates little change in the burning rate with hydrocarbon molecular weight, while the measurements show a monatonically decreasing burning rate with increasing molecular weight. Furthermore, as in the present investigation, the theory considerably overestimates the burning rate when the log mean temperature is used to evaluate gas phase properties.
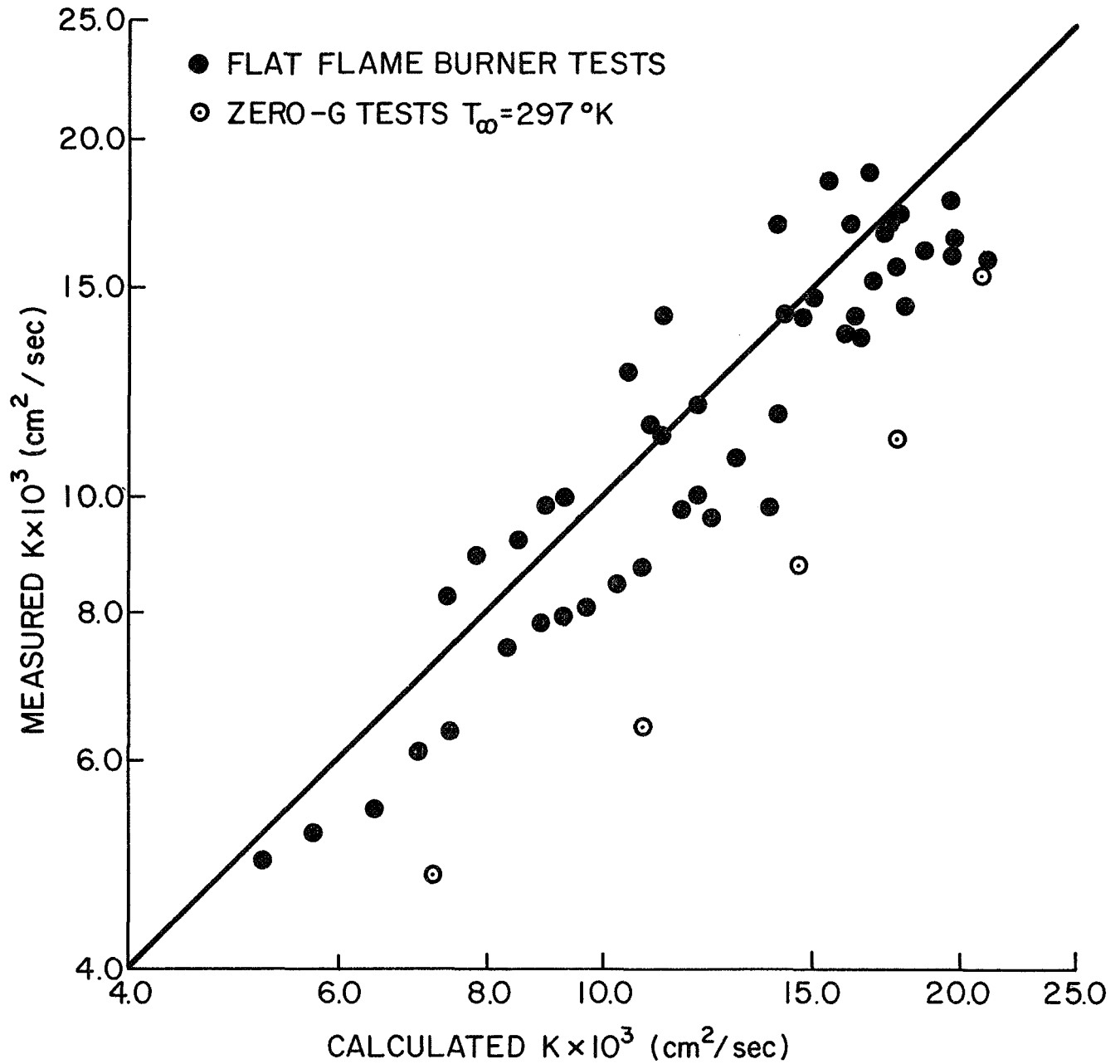
Fig. 15   Comparison of Computed (Method B) and Measured Burning Rate Constants for all Test Conditions.

TABLE III: THEORETICAL AND EXPERIMENTAL RESULTS FROM HOTTEL, ET AL[3]
ON THE BURNING RATES OF HEAVIER PARAFFINS

Fuel	Formula	Measured $M/4\pi r_\ell$	Predicted $M/4\pi r_\ell$
Cetane	$C_{16}H_{34}$	$6.1 \times 10^{-6} \frac{gmol}{sec\ cm}$	$22.6 \times 10^{-6} \frac{gmol}{sec\ cm}$
Eicosane	$C_{20}H_{42}$	5.7	22.1
Wax (n-hexacosane?)	$C_{26}H_{54}$	4.7	21.7

Thus the failure with molecular weight appears to be real, and not just a characteristic of the present experimental technique. In the following, the possible role of variable properties and gas phase fuel decomposition will be considered as possible explanations of this phenomena.

With increasing fuel molecular weight, properties such as ρD, etc. have an increasing variation in the gas phase. This could cause a systematic error with increasing fuel molecular weight for the present constant property solution.

Variable property effects are most easily examined for the case of negligible ambient oxygen concentration. This is acceptable since Fig. 13 shows that the oxygen concentration does not exert a strong influence on the trends with respect to molecular weight.

The analysis assumes quasi-steady spherically symmetric flow, liquid phase insolubility of the ambient gas, no decomposition of the fuel and steady evaporation at the wet bulb temperature of the droplet. For these conditions the energy equation takes the following form[12]

$$\lambda r^2 \frac{dT}{dr} = \dot{m} \, (h_F - h_{F\ell} + h_{fg}) \tag{40}$$

subject to the boundary conditions

$$r = r_\ell \, , \quad T = T_\ell; \quad r \to \infty, \quad T = T_\infty \tag{41}$$

The burning rate constant is given by the following equation,

$$K = 8\dot{m}/r_\ell \rho_\ell \tag{42}$$

At this limiting condition, gas phase diffusion characteristics (with their possible molecular weight effect) may influence the solution in two ways. First of all, λ may depend on the local composition as well as the temperature. However, the property relations in the Appendix show that it is a very good assumption to neglect the effect of composition on λ, since the thermal conductivity of the heavier hydrocarbons is almost identical to that of the ambient gas.

Secondly, the diffusion characteristics influence the value of the fuel mass fraction at the droplet surface for steady evaporation. This, in turn, affects the liquid temperature, ρ_ℓ and h_{fg} through the Clausius - Clapeyron relation. However, this effect is not large at moderate pressures, due to the non-linearity of the Clausius - Clapeyron relation. For most materials, rather small liquid temperature variations cause rather large composition changes. Therefore, with little error, T_ℓ may be taken as the boiling point temperature (with ρ_ℓ, h_{fg}, etc. also evaluated at the boiling point).[10]

With these assumptions, Eqs. (40) to (42) may be solved for the burning rate constant without considering the solution of the diffusion equations. Goldsmith and Penner,[4] have presented a fairly realistic variable property solution of this problem. They make the following assumptions with regard to the temperature dependence of λ and Cp_F.

$$\lambda = \lambda_\ell \ (T/T_\ell)$$
(43)

$$Cp_F = a + bT \ \bullet$$
(44)

The solution of the equations then yields the following expression for the burning rate constant[4]

$$K_{VP}^{*} = \frac{8\lambda_\ell}{\rho_\ell \ b \ T_\ell^{\circ}} \left[\ln\left\{ 1 + \frac{(T_\infty - T_\ell)}{h_{fg}} \ [a + \frac{b}{2}(T_\infty + T_\ell)] \right\} - \frac{a}{\xi} \ x \right.$$

$$\left. \ln\left\{ \frac{(a + bT_\infty - \xi)(a + bT_\ell + \xi)}{(a + bT_\infty + \xi)(a + bT_\ell - \xi)} \right\} \right]$$
(45)

where

$$\xi = \{a^2 - 2b \{h_{fg} - a \ T_\ell\} - \frac{b}{2} \ T_\ell^{2})\}^{1/2} \ \bullet$$
(46)

This solution has been compared with the present constant property solution for heptane and hexadecane evaporation at an ambient temperature of 2530°K. The physical parameters employed in the variable property calculation are tabulated in Table IV. These parameters were evaluated from the physical property correlations given in the Appendix.

TABLE IV: PHYSICAL PARAMETERS EMPLOYED IN THE VARIABLE PROPERTY CALCULATIONS

FUEL	$T_\ell \, °K$	$h_{fg} \, \frac{cal}{gm}$	$\rho_\ell \, \frac{gm}{cm^3}$	$\lambda_\ell \, \frac{cal}{cm \ sec \ °K}$	$a \, \frac{cal}{gm°K}$	$b \, \frac{cal}{gm°K^2}$
N-HEPTANE	372	75.6	.611	73×10^{-6}	.44	$.4 \times 10^{-3}$
N-HEXADECANE	560	54.2	.569	110×10^{-6}	.44	$.4 \times 10^{-3}$

TABLE V: COMPARISON OF VARIABLE AND CONSTANT PROPERTY CALCULATIONS

FUEL	$T_\infty \, °K$	$V_\infty \, \frac{cm}{sec}$	$p \ atm.$	$K^{*}_{VP} \, \frac{cm^2}{sec}$	$K_{VP} \, \frac{cm^2}{sec}$	$K \, \frac{cm^2}{sec}$
N-HEPTANE	2530	62.5	1.0	9.7×10^{-3}	10.9×10^{-3}	10.2×10^{-3}
N-HEXADECANE	2530	62.5	1.0	12.3×10^{-3}	13.7×10^{-3}	12.9×10^{-3}

Table V shows the computed results for the variable and constant property solutions. The difference between the two methods amounts to about 6% for these conditions. Therefore, in this case, the simpler constant property solution gives an adequate representation of variable property effects.

These results indicate that a realistic variable property solution also exhibits the same failure with respect to increasing fuel molecular weight as the constant property solution. Therefore, the inclusion of variable properties does not provide an explanation of the failure of the theory for the larger fuel molecules.

The evaluation of gas phase fuel decomposition effects can only be under taken qualitatively due to the great complexity of these processes. Even for relatively simple molecules like methane and ethane, many aspects of the decomposition process are not fully understood.[28-32]

Some information is available on the rate of disappearance of the original molecule for the heavier hydrocarbons.[32,33] This data was obtained for the most part in pyrolysis experiments in the absence of oxygen and oxidation products. Therefore, since it is known that oxygen containing species can influence the decomposition process,[30-32] the results are only qualitatively correct when applied to the present experiment.

If decomposition effects are to influence droplet evaporation rates, two factors must be satisfied. First of all, the reaction must be fast enough to cause significant decomposition of the fuel as it diffuses from the droplet toward the ambient flow. Secondly, the energy requirements of the decomposition process must act to reduce the heat flux, and thus the evaporation rate, at the droplet surface. Both requirements are met if the fuel reacts endothermically at temperatures well below the ambient temperature (for evaporation) or the flame temperature (for combustion).

The ratio of the characteristic diffusion time (fuel residence time in the boundary layer) and the characteristic chemical reaction time provides a convenient measure of the extent of reaction. When the parameter is large, it is implied that significant reaction takes place. In the absence of convection, this parameter takes the form kr_ℓ^2/D.

For present purposes, it is satisfactory to assume that the initial decomposition is first order,[30, 32] although in certain ranges a more complicated pressure dependence may be observed.[31] Under this assumption, specific rate constants are given by Griswold,[32] for a number of paraffin hydrocarbons. Although this data is old, more recent measurements for a more limited number of substances, given in Ref. 30, are in reasonably good agreement with the earlier work.

Using the data given in Ref. 32, and diffusion coefficients computed in the Appendix, the order of magnitude of $r_\ell^2 k/D$ was computed for a 1000μ diameter droplet. The results may be tabulated as follows:

Fuel	$\sigma(kr_\ell^2/D)$
Methane	10-5
Ethane	10-2
Propane	10-1
Hexane	1
Gas oil	10

The value of kr_ℓ^2/D varies very strongly with temperature. A gas temperature of 1300°K was used in the tabulation, as a typical average temperature in the boundary layer for the present test conditions. The decomposition characteristics of gas oil was taken as representative of the heavier hydrocarbons due to the absence of other data.

The tabulation shows that there is a progressive increase in the speed of the initial decomposition reaction as the molecular weight of the fuel increases. The magnitudes of the numbers are questionable, but as they stand, the heavier hydrocarbons would be expected to undergo significant decomposition for these conditions.

Similar results would also be obtained for conditions in many combustion chambers. The droplet sizes in sprays are generally smaller than 1000μ. However, this can be offset by combustion chamber pressures greater than one atmosphere. For example, the tabulation would be essentially the same for 300μ droplets at 10 atm., and decomposition effects would become even more important at higher pressures.

Following the initial decomposition, a large number of intermediate species are formed, making the specification of an overall reaction very difficult. In the absence of any oxygen, equilibrium thermodynamic calculations indicate that CH_4, C_2H_2, C_2H_4, H_2, C_2H, H and solid carbon are major product species at temperatures in the range 1000 - 2500°K.[34]

While there is disagreement concerning the details of hydrogen decomposition and carbon formation, it is generally agreed that unsaturated hydrocarbons and radicals are formed by thermal cracking and dehydrogenation. Radical recombination becomes important in the later stages, forming very large polymeric molecules which with increasing molecular weight, and continuing dehydrogenation, approach the properties of carbon.[28,29] These general characteristics have been observed in shock tube studies,[34] as well as in detailed probing of gaseous diffusion flames.[35]

In order to estimate whether such reactive processes could cause a significant reduction in evaporation rates it is necessary to simplify both the effective overall mechanism and the specific reaction rate. While many materials are involved, yields of acetylene and hydrogen are high for temp-

eratures greater than 1000°K. Since the formation of these materials is quite endothermic, these decomposition products will be considered in the following discussion. Another interesting limit is to assume that the final products are hydrogen and solid carbon, although the formation of solid carbon occurs much more slowly than the initial decomposition.[33]

With regard to the reaction rate, an upper bound to the thermal effect is obtained if it is assumed that the reaction takes place at the droplet surface. Under these conditions, the energy of decomposition becomes a part of the total energy of gasification, h_{fg}. Taking the case of negligible ambient oxygen concentration and also assuming that gas phase properties are constant, the following expression may be obtained for the dimensionless steady evaporation rate.[12]

$$\frac{\dot{m}\,Cp}{\lambda\,r_\ell} = \ln\left\{1 + \frac{Cp\,(T_\infty - T_\ell)}{h_{fg}}\right\} \tag{47}$$

At atmospheric pressure, h_{fg} = 54.3 cal/gm for n-hexadecane in the absence of decomposition. Assuming decomposition at the surface, h_{fg} = 2350 cal/gm if acetylene and hydrogen are the major products; and h_{fg} = 300 cal/gm if solid carbon and hydrogen are taken as the products. With $Cp\,(T_\infty - T_\ell)$ taken as 2000 cal/gm, a typical value for the present investigation, the RHS of Eq. (47) becomes 3.64 for no decomposition, 2.04 for carbon as the product and .62 for acetylene as the product. These results indicate that decomposition can cause a significant reduction in evaporation rates. Naturally, these changes are upper bounds and the effect would be smaller when reaction is distributed throughout the gas phase.

From this discussion, it appears that decomposition effects have greater promise than variable property effects as the mechanism causing difficulties with the theory for heavier hydrocarbons. Chemical reaction rates appear to be fast enough for the heavier hydrocarbons, and the energy requirements of some of the steps are sufficiently endothermic to cause a significant

reduction of the evaporation rate. Certainly further study of this phenomena appears to be warranted if reliable methods of computing droplet lifetimes are to be obtained for high pressure combustion systems, particularly those using high molecular weight fuels.

DROPLET LIFETIMES

The use of Eqs. (11), (18) and (23) to give instantaneous heat and mass transfer rates at the droplet presupposes the presence of an active combustion zone. Thus, for this formulation to be appropriate during the heat-up period, the time of gas phase ignition must be short in comparison to the heat-up time of the droplet.

For very small droplets at low ambient temperatures and pressures, ignition can occur late in the gasification period of the droplet (or not at all). Experiments conducted in air at atmospheric pressure by Kobayasi[9] and Nishiwaki[36] show this type of behavior. Gas temperatures in these tests were in the range 670 - 1000°K and the results indicate that ignition occurred some time after the initial heat-up period of the droplet.

More extensive testing by Faeth and Olson,[37] indicates that the time of ignition is not particularly related to the end of the heat-up period, but is a complicated function of droplet diameter, ambient temperature, ambient pressure and fuel type. In general, high ambient temperatures and pressures and large droplet diameters favor ignition early in the heat-up period.[37]

Extrapolation of the results of Ref. 37 to the present test conditions indicate droplet ignition should occur very early in the heat-up period. This estimation was checked experimentally by observing the time when a luminous zone appeared around the droplet, following its immersion in the hot burner gas. For these tests, dark field cine photographs were taken of the droplet. The camera was operated at approximately 150 pictures per second using Tri-X negative film.

The measured time of the appearance of luminosity for a variety of conditions is tabulated in Table VI. It should be noted that these results probably only represent an upper bound for the time required to establish an active combustion zone. For the more volatile fuels, luminousity was observed

TABLE VI: RATIO OF TIME OF LUMINOSITY TO HEAT-UP TIME

FOR VARIOUS HYDROCARBONS, $T_\infty = 2530\,^\circ K$, $V_\infty = 62.5$ cm/sec.

FUEL	$Y_x = 0.0455$			$Y_x = 0.2269$			$Y_x = 0.3713$		
	$d_{\ell o}$ (μ)	τ_i (sec)	τ_i/τ_H	$d_{\ell o}$ (μ)	τ_i (sec)	τ_i/τ_H	$d_{\ell o}$ (μ)	τ_i (sec)	τ_i/τ_H
N-HEPTANE	1412	.013	0.089	1366	.013	0.152	1318	.013	0.206
ISO-OCTANE	1348	.013	0.086	1418	.006	0.065	1450	.006	0.081
N-DECANE	1575	.025	0.093	1548	.019	0.110	1533	.013	0.099
HEXADECANE	1366	.300	0.143	1566	.270	0.097	1600	.230	0.143

τ_i — OBSERVED TIME OF IGNITION (sec)

τ_H — COMPUTED HEAT-UP TIME (sec)

one or two frames after the immersion of the droplet in the high temperature gas causing a large uncertainity in the actual time of luminosity. A second factor, particularly evident for the less volatile fuels, was that the intensity of the luminousity increased gradually as the droplet continued to heat up, as opposed to an abrupt appearance of luminousity typical of many ignition processes. This suggests that luminousity was detected when the fuel concentration, and thus droplet temperature, was high enough to give light of enough intensity to expose the film. Therefore, an active combustion zone may have been present some time before its actual detection as a luminous zone on the film.

Table VI also lists the ratio of the time of luminousity to the heat-up time of the droplet. The heat-up time was computed by method B, as the time required for the droplet to complete 95% of the temperature rise to the wet bulb state. In order to be conservative, these computations assumed the presence of an active combustion zone throughout the heat-up period since this assumption gives the minimum heat-up time.

The ratio of the time of luminousity to the heat-up time shown in Table VI indicates that combustion effects appear quite early for the conditions of these tests. Particularly in view of the fact that the measured ratio is only an upper bound. Therefore, it appears reasonable to assume that an active combustion zone was present throughout the lifetime of the droplet, for these high ambient temperature conditions.

Comparisons of theoretical and experimental life histories for n-heptane, n-decane and n-hexadecane droplets are shown in Figs. 16, 17, and 18 for two different ambient oxygen concentrations. The predictions are based on method B, allowing for liquid phase property variations with time.
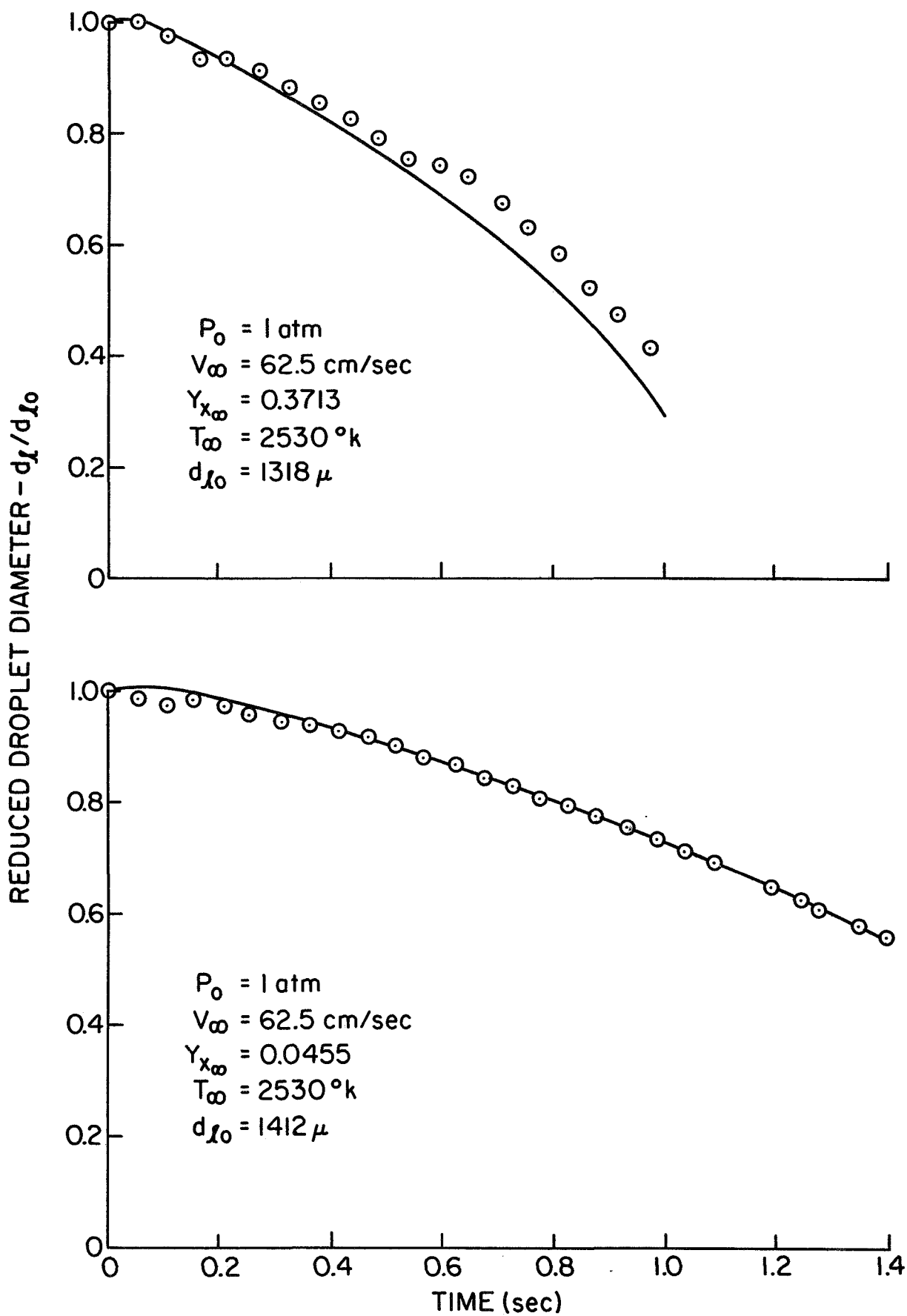
Fig. 16   n-Heptane Droplet Life Histories at Various Ambient Oxygen
Concentrations.
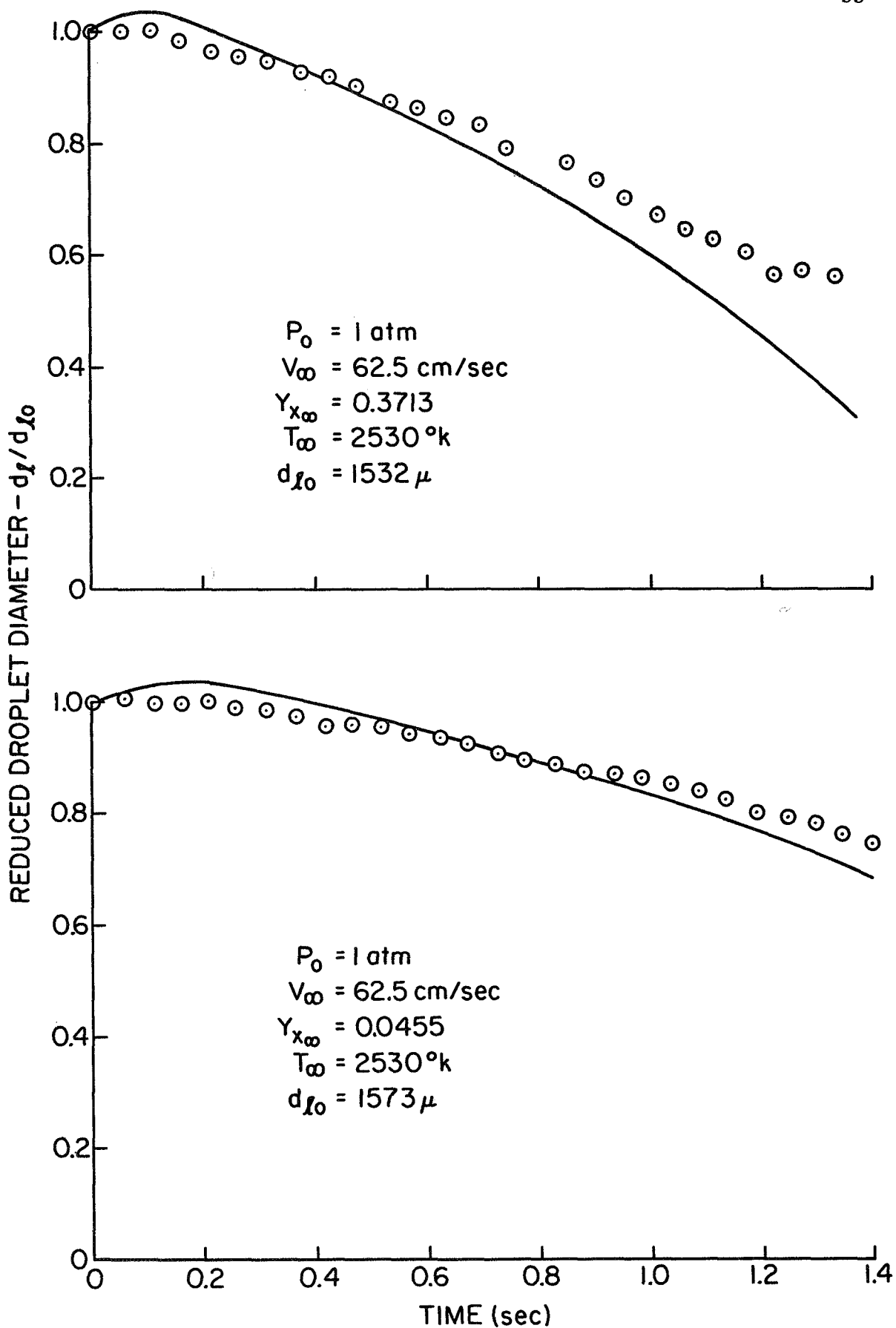
Fig. 17   n-Decane Droplet Life Histories at Various Ambient Oxygen Concentrations.
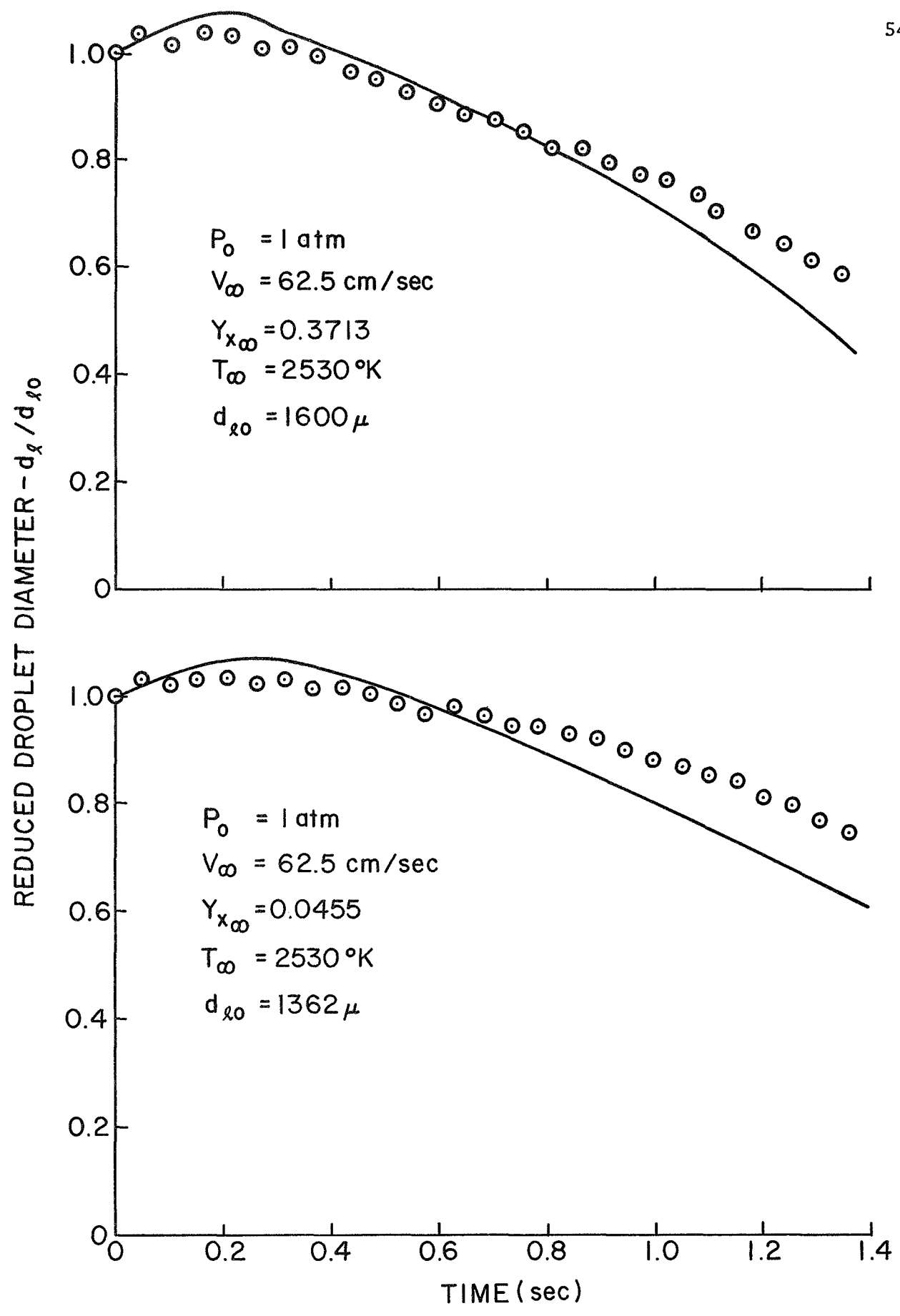
Fig. 18   n-Hexadecane Droplet Life Histories at Various Ambient Oxygen Concentrations.

In general, the results are quite good for n-heptane, with the quality of the prediction progressively decreasing for the heavier hydrocarbons. This behavior is perhaps to be expected, since the theory gives a good prediction of steady burning rate of n-heptane due to a fortuitous crossing of the theoretical and experimental burning rate curves at this point (Fig. 14). For the heavier hydrocarbons, the theory progressivley overestimates the burning rate (Fig. 14), which is reflected in the poorer lifetime predictions for n-decane and n-hexadecane (Figs. 17 and 18).

As the fuel volatility decreases, the temperature of the liquid at the wet bulb state increases. Due to the reduction in liquid density with increasing temperature, this causes increased swelling of the droplet during the heat-up period for the heavier hydrocarbons.

The theory is seen to overestimate the degree of swelling for all three fuels. This is probably due to the assumption of a uniform droplet temperature at each instant of time. It has been established for these test conditions that there are significant temperature gradients within the droplet during the heat-up period.[23] A transient analysis of the temperature distribution in the liquid phase acts both to reduce the degree of swelling for given surface temperature and to shorten the time required for the droplet surface to reach temperature levels near the wet bulb state.[23,24] Both of these effects act to reduce the predicted droplet diameter at any time during the heat-up period. Therefore, a complete transient analysis should yield a better prediction of the droplet diameter variation in the early stages of combustion, but with a rather large increase in computational complexity.

The experimental results show that the length of the heat-up period is reduced as the ambient oxygen concentration is increased. The theory models this effect reasonably well. This phenomena is best illustrated with n-hexadecane, Fig. 18, since the higher wet bulb temperature of this fuel extends the length of the heat-up period.

SUMMARY AND CONCLUSIONS

The present investigation has considered the heat-up and steady burning of a variety of fuel droplets in a flowing combustion gas environment. The data obtained in this investigation should be useful in checking analytical models for combustion chamber performance calculations since the present experiment provides a reasonably good simulation of combustion chamber conditions.

A simplified theoretical model was developed which yields an estimation of droplet heat and mass transfer rates during heat-up as well as at the steady burning condition. This solution divides the gas phase into regions interior and exterior of the reaction zone with constant average properties in each region. The model gave the best results when properties were evaluated at the log mean average temperature and average composition in each region, with an effective heat of reaction allowing for dissociation, no assumption of unity Lewis number and convection correlated on the basis of approach conditions.

The constant average property solution was compared with the variable property solution given by Goldsmith and Penner,[4] for the case of steady evaporation with a negligible ambient oxygen concentration. The two methods were found to agree within a few percent.

Comparison of the theory with experimental steady burning results showed reasonably good agreement for the lighter hydrocarbons. However, with increasing hydrocarbon molecular weight, the theory progressively over-estimates the burning rates with errors as high as 40% for n-hexadecane. Qualitative calculations indicate that fuel decomposition between the droplet surface and the oxidation zone (or the ambient gas in the case of evaporation

without combustion) might be the cause of this behavior. Further testing at higher pressures should help to resolve this question since decomposition effects are more important under these conditions.

Luminousity was observed very early in the heat-up period of the droplet for the present test conditions. Therefore in analyzing the droplet lifetime data, the assumption was made that an active combustion zone was present throughout the life of the droplet, i.e., negligible ignition delay. The validity of this assumption under complete combustion chamber conditions, where droplet sizes are smaller and initial relative velocities are higher than those of the present investigation requires further examination.

The comparison between theoretical and experimental droplet life histories was similar to the burning rate results. The prediction was reasonably good for the lighter hydrocarbons, but the quality of the solution progressively deteriorated with increasing fuel molecular weight. The results also suggested that a complete transient analysis of the temperature distribution in the liquid phase would improve the solution during the heat-up period. Unfortunately, a complete transient solution for the liquid phase would also greatly complicate system calculations for estimating combustion chamber performance.

REFERENCES

1. Spalding, D. B., "The Combustion of Liquid Fuels," Fourth Symposium (International) on Combustion, Williams and Wilkins, 1953, pp. 847-864.

2. Godsave, G. A. E., "Studies of the Combustion of Drops in a Fuel Spray," Ibid, pp. 818-830.

3. Hottel, H. C., Williams, G. C., and Simpson, H. C., "Combustion of Droplets of Heavy Liquid Fuels," Fifth Symposium (International) on Combustion, Reinhold, 1954, pp. 101-129.

4. Goldsmith, M. and Penner, S. S., "On the Burning of Single Drops of Fuel in an Oxidizing Atmosphere," Jet Propulsion, vol. 24, No. 4, 1954, pp. 245-251.

5. Goldsmith, M., "Experiments on the Burning of Single Drops of Fuel," Jet Propulsion, vol. 26, No. 3, 1956, pp. 172-178.

6. Wood, B. J., Rosser, W. A., and Wise, H., "Combustion of Fuel Droplets," AIAA Journal, vol 1, 1963, pp. 1076-1081.

7. Friedman, R. and Maček, A., "Ignition and Combustion of Aluminum Particles in Hot Gases," Combustion and Flame, vol. 6, no. 1, March, 1962, pp. 9-19.

8. Jones, W. H. (Chairman), "JANAF Thermochemical Tables," Dow Chemical Company, Midland, Michigan.

9. Kobayasi, K., "An Experimental Study of the Combustion of a Fuel Droplet," Fifth Symposium (International) on Combustion, Reinhold, 1954, pp. 141-148.

10. Williams, F. A., "On the Assumptions Underlying Droplet Vaporization and Combustion Theories," Journal of Chemical Physics, vol. 33, no. 1, 1960, pp. 133-144.

11. Priem, R. J. and Heidmann, M. F., "Propellant Vaporization as a Design Criterion for Rocket Engine Combustion Chambers," NASA Technical Report R-67, 1960.

12. Williams, F. A., Combustion Theory, Addison-Wesley, Reading, Massachusetts, 1965, Chapter 1.

13. Ibid, pp. 56-57.

14. Eisenklam, P., Arunachalam, S. A., and Weston, J. A., "Evaporation Rates and Drag Resistance of Burning Drops," Eleventh Symposium (International) on Combustion, The Combustion Institute, 1967, pp. 715-728.

15. Frössling, N., "Uber die Verdunstung fallender Tropfen," Beitrag. Geophys, vol. 52, 1938, pp. 170-216.

16. Fendell, F. E., Sprankle, M. L. and Dodson, D. S., "Thin-flame Theory for a Fuel Droplet in Slow Viscous Flow," J. Fluid Mechanics, vol. 126, part 2, 1966, pp. 267-280.

17. Fendell, F. E., "Decompositional Burning of a Droplet in a Small Peclet Number Flow," AIAA Journal, vol. 6, no. 10, 1968, pp. 1946-1953.

18. Rosner, D. E., Personal Communication, 1968.

19. Ranz, W. E. and Marshall, W. R., "Evaporation from Drops," Chem. Eng. Progress, vol. 48, 1952, Part I, pp. 141-146, Part 2, pp. 173-180.

20. Yuge, T., "Experiments on Heat Transfer from Spheres Including Combined Natural and Forced Convection," ASME Transactions, vol. 82, series C, 1960, pp. 214-220.

21. Acrivos, A., and Taylor, T. D., "Heat and Mass Transfer from Single Spheres in Stokes Flow," Physics of Fluids, vol. 5, no. 4, 1962, pp. 387-394.

22. Allender, C., "Untersuchung des Absorptions --- vorganges in Absorbenten- shichten mit Linearer Absorptionsisotherme," Trans. Royal Institute of Technology, Stockholm, no. 70, 1953.

23. Faeth, G. M., "On the Prediction of Monopropellant Droplet Life Histories," AIAA Paper No. 69-563, 1969.

24. Sotter, J. G., "Nonsteady Evaporation of Liquid Propellant Drops: The Grossman Model," JPL Technical Report 32-1061, 1968.

25. Hall, A. R., "Experimental Temperature Gradients in Burning Drops," Seventh Symposium (International) on Combustion, Butterworths, London, 1959, pp. 399-406.

26. Combs, R. L. Discussion of Ref. 14, Ibid, pp. 727-728.

27. Faeth, G. M., Dominicis, D. P., Tulpinsky, J. F., and Olson, D. R., "Super- critical Bipropellant Droplet Combustion," Twelfth Symposium (Inter- national) on Combustion, The Combustion Institute, Pittsburgh, Pa., 1969, pp. 9-18.

28. Gordon, A. S., "A Review of the Kinetics and Mechanism of the Pyrolysis of Hydrocarbons," Fifth AGARD Combustion Colloquium, MacMillan Company, New York, 1963, pp. 111-134.

29. Palmer, H. B. and Cullis, C. F., "The Formation of Carbon from Gases," The Chemistry and Physics of Carbon, P. L. Walker (Ed.) vol. 1, Marcel Dekker, Inc. 1965, pp. 265-325.

30. Minkoff, G. J. and Tipper, C. F. H., Chemistry of Combustion Reactions, Butterworths, London, 1962, pp. 237-257.

31. Benson, S. W., The Foundations of Chemical Kinetics, McGraw-Hill, 1960, pp. 343-363.

32. Griswold, J., Fuels, Combustion and Furnaces, McGraw-Hill, New York, 1946, pp. 163-165.

33. Glick, H. S., "Shock Tube Studies of Reaction Kinetics of Aliphatic Hydrocarbons," Seventh Symposium (International) on Combustion, Butterworths, London, 1958, pp. 98-107.

34. Kroepelin, H. "Calculation of Equilibria of Hydrocarbons Heated to High Temperatures, Intensely Heated Air, and Temperature Measurements in Electric Arcs," 5th AGARD Combustion Colloquium, MacMillan Company, New York, 1963, pp. 45-60.

35. Gordon, A.S., Smith, S.R., and McNesby, J.R., "Study of the Chemistry of Diffusion Flames," Seventh Symposium (International) on Combustion, Butterworths, London, 1958, pp. 317-324.

36. Nishiwaki, N., "Kinetics of Liquid Combustion Processes: Evaporation and Ignition Lag of Fuel Droplets," Fifth Symposium (International) on Combustion, Reinhold, 1954, pp. 148-158.

37. Faeth, G. M. and Olson, D. R., "Spontaneous Ignition of Motionless Fuel Droplets," S.A.E. Transactions, 1969 Paper No. 680465, pp. 1793-1802.

38. Tarifa, C. S., del Notario, P. P. and Moreno, F. G., "Combustion of Liquid Monoporpellants and Bipropellants in Droplets," Eighth Symposium (International) on Combustion, Williams and Wilkins, Baltimore, 1962, pp. 1035-1056.

39. Reid, R. C., and Sherwood, T. K., The Properties of Gases and Liquids, McGraw-Hill, New York, Second Edition, 1966.

40. Wilke, C. R., "Diffusional Properties of Multicomponent Gases," Chem. Eng. Progress, vol. 46, no. 2, 1950, pp. 95-104.

41. Rossini, F. D., "Selected Values of the Physical and Thermodynamical Properties of Hydrocarbons and Related Components," American Petroleum Institute, Carnegie, 1953.

42. Maxwell, J. D., Data Book on Hydrocarbons, Van Nostrand, New York, 1950.

43. Svehla, R. A., "Estimated Viscosities and Thermal Conductivities of Gases at High Temperatures, NASA Technical Report R-132, 1962.

44. International Critical Tables, McGraw-Hill Book Company, New York, 1926-1930.

45. Stull, D. R., "Vapor Pressure of Pure Substances, Organic Compounds," Industrial and Engineering Chemistry, vol. 39, no. 4, April, 1947, pp. 517-540.

Appendix A: Physical Properties

A1. Gas Phase Properties

Thermal conductivity and specific heat

The gas phase thermal conductivities and specific heats were correlated with the following equations

$$\lambda = C_1 + C_2 T \qquad \text{(BTU/hr ft °R)} \qquad \text{(A-1)}$$

$$Cp = C_3 + C_4 T \qquad \text{(BTU/lbm °R)} \qquad \text{(A-2)}$$

where temperature is in degrees Rankine. The constants in Eqs. (A-1) and (A-2) are tabulated in Table VII. The combustion products are treated as a single species whose properties are averaged for an equimolar mixture of carbon dioxide, nitrogen and water vapor.

Density

The ideal gas equation was used to compute gas density.

$$\rho = p \, W/R_u T \qquad \text{(A-3)}$$

The molecular weight was computed for the average composition of each region. The temperature was taken to be the log mean average temperature in each region.

Diffusion Coefficient

Effective diffusion coefficients for Regions A and B were computed according to a method derived by Wilke (40) for fuel diffusing through the combustion products in Region A and oxygen diffusing through combustion products in Region B. Binary diffusion coefficients for the diffusing species and each of the other species required by this method were computed by the Slattery-Bird correlation as given in Reference (39). The resulting correlations are given as,

TABLE VII: Constants in Equations A1 and A2

| Component | $C_1 \times 10^3$ | $C_2 \times 10^6$ | T < 1000°R | | 1000 <T< 1700°R | | T > 1700°R | |
			C_3	$C_4 \times 10^3$	C_3	$C_4 \times 10^3$	C_3	$C_4 \times 10^3$
Methane	0	55.4	0.310	0.432	0.312	0.428	0.598	0.260
Propane	0	39.0	0.103	0.566	0.312	0.358	0.564	0.210
N Pentane	-6.6	28.5	0.085	0.575	0.318	0.342	0.586	0.185
N Heptane	-6.06	26.75	0.094	0.556	0.3185	0.338	0.600	0.176
N Octane	-6.42	27.0	0.095	0.554	0.3136	0.340	0.605	0.170
Iso Octane	-6.42	27.0	0.095	0.554	0.3136	0.340	0.605	0.170
N Decane	-6.60	26.3	0.097	0.550	0.314	0.336	0.585	0.175
N Tridecane	-7.40	26.0	0.084	0.567	0.322	0.328	0.608	0.160
N Hexadecane	-7.46	26.0	0.0935	0.548	0.3126	0.333	0.619	0.160
Methanol	-15.2	47.7	0.236	0.264	0.450	0.136	0.819	0.062
Ethanol	-28.0	60.0	0.163	0.392	0.305	0.205	0.543	0.110
Butanol	-30.0	64.0	0.140	0.430	0.270	0.300	0.542	0.140
Heptanol	-26.0	47.0	0.120	0.390	0.120	0.390	0.644	0.080
Decanol	-22.0	48.0	0.100	0.500	0.286	0.314	0.548	0.160
Oxygen	11.0	17.78	0.2248	0.019	0.2248	0.019	0.2248	0.019
Combustion Products	0	26.5	0.2612	0.043	0.2612	0.043	0.2612	0.043

$$D_A = \frac{(T/1.8)^{2.334}/P}{C_1 + C_2 \, (T/1.8)^{0.511}} \qquad ft^2/hr \qquad (A-4)$$

and

$$D_B = \frac{(T/1.8)^{2.334}/P}{C_3 + C_4 \, (T/1.8)^{0.511}} \qquad ft^2/hr \qquad (A-5)$$

The constants are tabulated on Table VIII. Temperatures are in degrees Ranking and pressures in atmospheres.

A2. Liquid Phase Properties

Density

$$\rho_\ell = C_1 - C_2 \, T_\ell \qquad lbm/fT^3 \qquad (A-6)$$

Specific Heat

$$C_{p\ell} = C_3 + C_4 \, T_\ell \qquad BTU/lbm \; °R \qquad (A-7)$$

Heat of Vaporization

$$h_{fg} = C_5 \, (1 - T_r)^{0.38} \qquad BTU/lbm \qquad (A-8)$$

Vapor Pressure

$$P_v = C_6 \exp\left(\frac{-1}{T_\ell/C_7 - C_8}\right) \qquad atm \qquad (A-9)$$

The constants for the above equations are tabulated in Table IX. Critical temperatures used in the reduced temperature, T_r, of Eq. (A-8) are also given. Liquid temperatures in the above equations are in degrees Rankine.

Heat of Reaction

The standard heat of reaction was taken to be the lower heating value of the fuel. The effective heat of reaction was computed as the energy required to heat the combustion products (assumed to be H_2O and

TABLE VIII: CONSTANTS IN EQUATIONS A4 AND A5

Diffusing Component	C_1 x 10^{-5}	C_2 x 10^{-5}	C_3 x 10^{-4}	C_4 x 10^{-4}
Methane	2.104	0.274	20.351	2.940
Propane	3.745	0.563	17.444	3.197
N-Pentane	4.904	0.767	16.651	3.268
N-Heptane	5.880	0.933	16.281	3.301
N-Octane	6.316	1.006	16.161	3.311
Iso-Octane	6.041	0.973	16.161	3.311
N-Decane	7.127	1.140	15.990	3.326
N-Tridecane	8.190	1.311	15.829	3.341
N-Hexadecane	9.138	1.464	15.726	3.350
Methanol	4.306	0.458	20.351	2.940
Ethanol	4.439	0.571	18.316	3.120
Butanol	5.246	0.763	19.960	3.240
Heptanol	6.548	1.003	16.281	3.301
Decanol	7.335	1.160	15.990	3.326

Component	C_1	C_2 $\times 10^3$	C_3	C_4 $\times 10^3$	C_5	Tc (°R)	C_6	C_7	C_8 $\times 10^3$
Methane	36.1	48.4			281.0	343.0	1667.0	1612.0	7.83
Propane	52.8	40.0			305.0	666.0	8650.0	3365.0	13.39
N Pentane	56.4	32.8			231.0	845.6	9130.0	4410.0	16.78
N Heptane	58.8	30.5	0.223	0.590	212.0	972.3	10531.4	5255.9	19.3
N Octane	60.8	30.5	0.215	0.590	205.0	1024.9	11080.0	5616.5	20.45
Iso Octane	58.9	29.75	0.219	0.582	177.5	979.8	8536.5	5213.3	18.16
N Decane	60.05	27.5	0.275	0.568	192.0	1114.0	11780.0	6222.2	22.8
N Tridecane	62.8	28.4			180.0	1219.0	12300.0	6940.0	25.95
N Hexadecane	64.1	28.1	0.228	0.530	171.5	1305.0	14100.0	7590.2	28.2
Methanol	67.8	35.0			715.0	924.0	0.78×10^6	8280.0	0.0
Ethanol	65.6	31.0			570.0	922.0	1.732×10^6	9110.0	0.0
Butanol	62.3	22.5			400.0	1008.0	1.828×10^6	10100.0	0.0
Heptanol	63.3	23.0			301.0	1150.0	3.16×10^6	12000.0	0.0
Decanol	64.3	23.5			279.0	1180.0	1.282×10^6	12720.0	0.0

CO_2) from 298°K to the flame temperature for adiabatic combustion of the fuel with oxygen. The adiabatic flame temperature was computed, allowing for all relevant dissociation reactions. The thermochemical properties for these calculations were taken from Ref. 8, with the exception of the heat of formation of the fuel. The source for the heat of formation may be found in Table XII. The values of the standard and corrected heat of reaction are given in Table X.

A3   Ambient Gas Properties

For the ambient gas consisting of N components, the mixture properties were determined as follows:

Specific Heat

$$C_p = \sum_{i=1}^{N} X_i W_i Cp_i \Big/ \sum_{i=1}^{N} X_i W_i \qquad \text{(A-10)}$$

where

$$Cp_i = C_1 + C_2 T \qquad \text{BTU/lbm°R} \qquad \text{(A-11)}$$

Viscosity

$$\nu = \sum_{i=1}^{N} X_i \nu_i \qquad \text{(A-12)}$$

where

$$\nu_i = C_3 + C_4 T \qquad \text{lbm/ft sec} \qquad \text{(A-13)}$$

Thermal Conductivity

$$\lambda = \sum_{i=1}^{N} X_i \lambda_i \qquad \text{(A-14)}$$

where

$$\lambda_i = C_5 + C_6 T \qquad \text{BTU/hr ft °F} \qquad \text{(A-15)}$$

TABLE X: HEATS OF REACTION

MATERIAL	STANDARD H_c (B/lbm)	CORRECTED H_c (B/lbm)
Methane	21500	11590
Propane	19930	10150
N-Pentane	19500	9840
N-Heptane	19300	9700
N-Octane	19250	9650
N-Decane	19175	9610
N-Tridecane	19080	9530
N-Hexadecane	19050	9500
Methanol	8580	5540
Ethanol	12800	6660
Butanol	14220	7680
Heptanol	17100	8270
Decanol	17000	8560

Density

$$\rho = P\Sigma_{i=1}^{N} X_i W_i / R_u T \qquad \text{lbm/ft}^3 \qquad (A-16)$$

Diffusion Coefficient

$$D = \frac{1 - X_1}{\sum_{j=2}^{N} (X_j / D_{1j})} \qquad (A-17)$$

where X_1 refers to the mole fraction of oxygen in the ambient gas mixture, X_j is the mole fraction of all other components in the mixture and D_{1j} is the diffusion coefficient for oxygen in component j. The D_{1j}'s were calculated from a Slattery-Bird correlation as:

$$D_{1j} = C_7 (T/1.8)^{1.823}/P \qquad \text{ft}^2/\text{sec} \qquad (A-18)$$

Under decomposition conditions when oxygen was not present in the ambient gas, the diffusion coefficient was not calculated and the Schmidt number was taken to be equal to the Prandtl number of the gas mixture.

The constants in Equations (A-10) to (A-18) are tabulated in Table XI. In the above equations, temperatures are in degrees Rankine and pressures in atmospheres.

A4   References for Physical Properties

Sources for physical properties are tabulated in Table XII.

TABLE XI: Constants in Equations A10 to A18

Component	C_1 $\times 10^3$	C_2 $\times 10^6$	C_3 $\times 10^7$	C_4 $\times 10^{10}$	C_5 $\times 10^3$	C_6 $\times 10^6$	C_7 $\times 10^{10}$
O_2	248.0	9.3	136.07	101.91	11.00	17.78	
O	282.0	9.3	124.3	93.33	17.40	17.20	
N_2	281.6	6.7	102.47	87.73	7.70	16.56	68.15
N_0	277.4	4.0	131.37	95.19	8.95	17.73	70.00
CO_2	298.0	7.5	102.47	87.73	2.88	18.75	51.30
CO	292.3	4.7	109.19	87.73	7.74	17.20	67.28
H_2O	583.0	29.4	91.60	97.30	-11.46	44.60	
H_2	3610.0	143.2	72.00	68.00	75.00	99.80	

TABLE XII: PROPERTY SOURCES AND METHODS

Material	Pe	Cp_e	H_{fg}	Pv	Hc	λ	Cp	μ	D
Paraffins	41	41	Eq. (A-8)	41	41	42	41	---	Eq.(A-4)
Methanol	44	--	↓	44	44	43[a]	39[b]	39[c]	↓
Butanol	44	--		44	44	43[a]	39[b]	39[c]	
Decanol	‡	--	↓	45	39[d]	43[a]	39[b]	39[c]	↓
Combustion and Ambient Gases (H_2, O_2, etc.)	--	--	--	--	--	43	43	43	Eq.(A-18)

a Computed, method of Ref. (43)

b Computed, Rihani and Doraiswamy method, Ref. (39)

c Computed, Stiel and Thodos method, Ref. (39)

d Computed, method of Souders, Matthews, and Hurd, Ref. (39)

† Measured in this laboratory (17 - 78° C)

REPORT DISTRIBUTION LIST OF

CONTRACT NO. NGR 39-009-077

Dr. R. J. Priem   MS 500-204 (4)
NASA Lewis Research Center
21000 Brookpark Road
Cleveland, Ohio   44135

Norman T. Musical
NASA Lewis Research Center
21000 Brookpark Road
Cleveland, Ohio 44135

Library   (2)
NASA Lewis Research Center
21000 Brookpark Road
Cleveland, Ohio 44135

Report Control Office
NASA Lewis Research Center
21000 Brookpark Road
Cleveland, Ohio   44135

NASA Representative (6)
NASA Scientific and Technical
    Information Facility
P. O. Box 33
College Park, Maryland   20740

V. Agosta
Brooklyn Polytechnic Institute
Long Island Graduate Center
Route 110
Farmingdale, New York 11735

B. P. Breen
Dynamic Science, a Division of
    Marshall Industries
1900 Walker Avenue
Monrovia, California 91016

Thomas J. Chew
AFRPL (RPPZ)
Edwards, California   93523

T. W. Christian
Chemical Propulsion Information Agency
8621 Georgia Avenue
Silver Spring, Maryland 20910

R. M. Clayton
Jet Propulsion Laboratory
Californai Institute of Technology
4800 Oak Grove Drive
Pasadena, California   91103

E. W. Conrad   MS 500-204
NASA Lewis Research Center
21000 Brookpark Road
Cleveland, Ohio   44135

Dr. E. K. Dabora
University of Connecticut
Aerospace Department
Storrs, Connecticut   06268

O. W. Dykema
Aerospace Corporation
P. O. Box 95085
Los Angeles, California   90045

G. W. Elverum
TRW Systems
1 Space Park
Redondo Beach, California   90278

R. Edse
Ohio State University
Department of Aeronautical and
    Astronautical Engineering
Columbus, Ohio   43210

G. D. Garrison
Pratt and Whitney Aircraft
Florida Research and Development
    Center
P. O. Box 2691
West Palm Beach, Florida   33402

M. Gerstein
Department of Mechanical Engineering
University of Southern California
University Park
Los Angeles, California   90007

I. Glassman
Princeton University
James Forrestal Research Center
P. O. Box 710
Princeton, New Jersey   08540

Richard W. Haffner
Air Force Office of Scientific
    Research
1400 Wilson Blvd.
Arlington, Virginia   22209

D. Harrje
Princeton University
James Forrestal Research Center
P. O. Box 710
Princeton, New Jersey   08540

T. Inouye   Code 4581
U. S. Naval Weapons Center
China Lake, California   93555

R. D. Jackel, 429
Office of Naval Research
Navy Department
Washington, D. C.   20360

R. B. Lawhead
Rocketdyne
A Division of North American
    Aviation
6633 Canoga Avenue
Canoga Park, California   91304

R. S. Levine, Code RPL
NASA Headquarters
6th and Independence Avenues, S. W.
Washington, D. C.   20546

Ted Male   MS 500-209
NASA Lewis Research Center
21000 Brookpark Road
Cleveland, Ohio   44135

J. M. McBride
Aerojet-General Corporation
P. O. Box 15847
Sacramento, California   95809

P. D. McCormack
Dartmouth University
Hanover, New Hampshire   03755

C. E. Mitchell
Colorado State University
Fort Collins, Colorado   80521

P. S. Myers
University of Wisconsin
Mechanical Engineering Department
1513 University Avenue
Madison, Wisconsin   53705

J. A. Nestlerode
Rocketdyne
A Division of North American
    Aviation
6633 Canoga Anenue
Canoga Park, California   91304

J. A. Nicholls
University of Michigan
Aerospace Engineering
Ann Arbor, Michigan   48104

James C. O'Hara
Tulane University
Department of Mechanical Engineering
New Orleans, Louisianna   70118

A. K. Oppenhiem
University of California
Department of Aeronautical Sciences
6161 Etcheverry Hall
Berkeley, California   94720

J. S. Osborn
Purdue University
School of Mechanical Engineering
Lafayette, Indiana   47907

Dr. K. Ragland
University of Wisconsin
Mechanical Engineering Department
Madison, Wisconson   53705

Dr. A. A. Ranger
Purdue University
School of Aeronautics, Astronautics,
    and Engineering Sciences
Lafayette, Indiana 47907

F. H. Reardon
Sacramento State College
School of Engineering
6000 J. Street
Sacramento, California 95819

B. A. Reese
Purdue University
School of Mechanical Engineering
Layafètte, Indiana 47907

R. J. Richmond R-Pand VE-PA
NASA George C. Marshall Space
    Flight Center
Huntsville, Alabama 35812

J. H. Rupe
Jet Propulsion Laboratory
California Institute of Technology
4800 Oak Grove Drive
Pasadena, California 91103

Dr. R. F. Sawyer
University of California
Mechanical Engineering, Thermal Systems
Berkeley, California 94720

K. Scheller
ARL (ARC)
Wright-Patterson AFB
Dayton, Ohio 45433

Roger A. Strehlow
University of Illinois
Aeronautical Engineering Department
Urbana, Illinois 61801

J. G. Thibadaux
NASA Manned Spacecraft Center
Houston, Texas 77058

T. P. Torda
Illinois Institute of Technology
Room 200 M.H.
3300 South Federal Street
Chicago, Illinois 60616

T. Y. Toong
Massachusetts Institute of Technology
Department of Mechanical Engineering
Cambridge, Massachusetts 02139

Richard Weiss
AFRPL
Edwards, California 93523

W. W. Wharton AMSMI-RKL
U. S. Army Missile Command
Redstone Arsenal, Alabama 35808

F. A. Williams
University of California
Aerospace Engineering Department
P. O. Box 109
LaJolla, California 92038

L. M. Wood
Bell Aerosystems Company
P. O. Box 1
Mail Zone J-81
Buffalo, New York 14205

B. T. Zinn
Georgia Institute of Technology
Aerospace School
Atlanta, Gerogia 30332

Office of Grants and Research
    Contracts   (10)
Office of Space Science and Applica-
    tions
Code SC
National Aeronautics and Space
    Administration
Washington, D. C. 20546